

UC Merced

UC Merced Previously Published Works

Title

Controls on timescales of soil organic carbon persistence across sub-Saharan Africa.

Permalink

<https://escholarship.org/uc/item/2qk876dq>

Journal

Global Change Biology, 30(1)

Authors

von Fromm, Sophie

Doetterl, Sebastian

Butler, Benjamin

et al.

Publication Date

2024

DOI

10.1111/gcb.17089

Peer reviewed

RESEARCH ARTICLE

Controls on timescales of soil organic carbon persistence across sub-Saharan Africa

Sophie F. von Fromm^{1,2}  | Sebastian Doetterl²  | Benjamin M. Butler³  |
 Ermias Aynekulu⁴  | Asmeret Asefaw Berhe⁵  | Stephan M. Haefele⁶  |
 Steve P. McGrath⁶ | Keith D. Shepherd^{6,7}  | Johan Six²  | Lulseged Tamene⁸  |
 Ebagnerin J. Tondoh^{9,10}  | Tor-Gunnar Vågøen⁴  | Leigh A. Winowiecki⁴  |
 Susan E. Trumbore¹  | Alison M. Hoyt¹¹ 

¹Max-Planck Institute for Biogeochemistry, Jena, Germany

²Department of Environmental Systems Science, ETH Zurich, Zurich, Switzerland

³The James Hutton Institute, Aberdeen, UK

⁴World Agroforestry Centre (ICRAF), Nairobi, Kenya

⁵University of California Merced, Merced, California, USA

⁶Rothamsted Research, Harpenden, UK

⁷Innovative Solutions for Decision Agriculture (iSDA), Harpenden, UK

⁸International Center for Tropical Agriculture (CIAT), Addis Ababa, Ethiopia

⁹Nangui Abrogoua University, Abidjan, Côte d'Ivoire

¹⁰CIFOR-ICRAF, Abidjan, Côte d'Ivoire

¹¹Stanford University, Stanford, California, USA

Correspondence

Sophie F. von Fromm, Dartmouth College, 78 College St, Hanover, NH 03755, USA.
 Email: sophie.von.fromm@dartmouth.edu

Present address

Sophie F. von Fromm, Dartmouth College, Hanover, New Hampshire, USA

Funding information

Bill and Melinda Gates Foundation, Grant/Award Number: 51353; Biotechnology and Biological Sciences Research Council, Grant/Award Number: BBS/OS/GC/000014B; H2020 European Research Council, Grant/Award Number: 695101; Institute Strategic Program (ISP), Grant/Award Number: BBS/E/C/00010310

Abstract

Given the importance of soil for the global carbon cycle, it is essential to understand not only how much carbon soil stores but also how long this carbon persists. Previous studies have shown that the amount and age of soil carbon are strongly affected by the interaction of climate, vegetation, and mineralogy. However, these findings are primarily based on studies from temperate regions and from fine-scale studies, leaving large knowledge gaps for soils from understudied regions such as sub-Saharan Africa. In addition, there is a lack of data to validate modeled soil C dynamics at broad scales. Here, we present insights into organic carbon cycling, based on a new broad-scale radiocarbon and mineral dataset for sub-Saharan Africa. We found that in moderately weathered soils in seasonal climate zones with poorly crystalline and reactive clay minerals, organic carbon persists longer on average (topsoil: 201 ± 130 years; subsoil: 645 ± 385 years) than in highly weathered soils in humid regions (topsoil: 140 ± 46 years; subsoil: 454 ± 247 years) with less reactive minerals. Soils in arid climate zones (topsoil: 396 ± 339 years; subsoil: 963 ± 669 years) store organic carbon for periods more similar to those in seasonal climate zones, likely reflecting climatic constraints on weathering, carbon inputs and microbial decomposition. These insights into the timescales of organic carbon persistence in soils of sub-Saharan Africa suggest that a process-oriented grouping of soils based on pedo-climatic conditions may be useful to improve predictions of soil responses to climate change at broader scales.

KEYWORDS

African Soil Information Service, Afrotropics, clay mineralogy, climate change, mean C age, radiocarbon, subtropical

This is an open access article under the terms of the [Creative Commons Attribution-NonCommercial](https://creativecommons.org/licenses/by-nc/4.0/) License, which permits use, distribution and reproduction in any medium, provided the original work is properly cited and is not used for commercial purposes.

© 2023 The Authors. *Global Change Biology* published by John Wiley & Sons Ltd.

1 | INTRODUCTION

Sub-Saharan Africa faces major environmental and societal challenges: Population is projected to grow from 1.2 billion today to 3.4 billion by 2100 (United Nations, 2022), which is expected to lead to further increases in deforestation and expansion of cropland (Hansen et al., 2013). Predicting associated changes in soil organic carbon (SOC) dynamics requires an understanding of the factors that control not only how much SOC is stored, but also for how long it is stored in soils, that is, the timescales of SOC persistence. There are many studies linking SOC content to vegetation, climate, and edaphic parameters, particularly soil mineralogy (Luo et al., 2021; Rasmussen, Heckman, et al., 2018; von Fromm et al., 2021; Yu et al., 2021), but there are fewer data on SOC age (here used as an indicator for SOC persistence) at broad spatial scales (Chen et al., 2021; Heckman et al., 2021). The available SOC data for sub-Saharan Africa suggest that about 24 Pg C is stored in the top five centimeters of soil (Hengl et al., 2015); more than twice the current annual global fossil CO₂ emissions (ca. 10 Pg C; Friedlingstein et al., 2022). On average, this SOC is estimated to persist in soil for a period of a few centuries, which is up to an order of magnitude shorter than SOC in other geographic areas (Shi et al., 2020).

Radiocarbon measurements ($\Delta^{14}\text{C}$) can be used to estimate the average time (years to millennia) since the C in soils was fixed from the atmosphere, including the time spent in plants (here defined as mean SOC age; Trumbore, 2009). Global meta-analyses of soil radiocarbon measurements have shown that the youngest mean SOC age (ca. 200–300 years) is usually found in warm and wet climates where both productivity and microbial activity are typically high (Mathieu et al., 2015; Shi et al., 2020). Soils with younger mean SOC ages exchange C more quickly with the atmosphere and are presumably more responsive to change, making the SOC less persistent. However, this assumption ignores the possibility that with climate change, environments with more persistent SOC (with older mean SOC age) may experience conditions where formerly persistent SOC becomes available to microbes and can be rapidly degraded; accelerating the C exchange between soil and atmosphere. Current global analyses of SOC dynamics typically suffer from a lack of data outside temperate regions, and this is especially true for deeply weathered soils from (sub-)tropical regions. Further, they tend to use general predictors that do not provide detailed insights into the underlying mechanisms driving differences in SOC content and age (Mathieu et al., 2015; Shi et al., 2020). Mineralogy is particularly known to affect SOC persistence, through its influence on soil structure and the provision of reactive mineral surfaces with different capacities for SOC sorption (Schmidt et al., 2011; Six, Feller, et al., 2002; Wattel-Koekkoek et al., 2003). In this context, fine-scale studies using carefully defined gradients have shown that SOC age increases with the amount of poorly crystalline minerals (Masiello et al., 2004; Rasmussen, Throckmorton, et al., 2018; Torn et al., 1997). These minerals are composed of Al and Fe oxyhydroxides and are characterized by large specific surface areas with a high proportion of reactive sites (Parfitt & Childs, 1988). For the same reason, soils with 2:1 clay minerals, such as smectite and vermiculite, are also known to yield older SOC compared to soils dominated by 1:1

clay minerals, such as kaolinite (Khomu et al., 2017; Wattel-Koekkoek et al., 2003) and can promote soil aggregation and occlusion of SOC (Six et al., 2000; Tisdall & Oades, 1982). However, Wattel-Koekkoek and Buurman (2004) observed no significant difference between the mean SOC age of kaolinite-bound and smectite-bound organic matter in soils from northern Mozambique. Additionally, cultivation can alter the timescales of SOC persistence (Six, Feller, et al., 2002), due to decreased C inputs and increased C decomposition (Harrison et al., 1993). While these studies have greatly improved our understanding of how the drivers of SOC persistence operate individually, it is necessary to increase the spatial scale of examination to reveal how they interact across contrasting geo-ecological environments. Similarly, the biogeochemical properties of tropical and subtropical soils relevant for SOC persistence can differ strongly from those of temperate soils due to differences in the pedogenetic development history. Thus, the present and future persistence of SOC in tropical and subtropical landscapes is subject to large uncertainties.

Here, we use a broad-scale approach to investigate drivers and factors that influence SOC persistence across sub-Saharan Africa. We present a comprehensive soil radiocarbon and mineral dataset, consisting of 510 new radiocarbon measurements (Figure 1a; Figure A1) from topsoils (0–20 cm) and subsoils (20–50 cm), each with accompanying climatic, mineralogical and land use information. Soil landscapes within sub-Saharan Africa are extremely diverse and have developed over varying amounts of time across contrasting parent materials and geo-climatic conditions. The data presented here are representative of these diverse landscapes in terms of the range of key climate and soil characteristics they cover, although parts of the inner tropics are missing (Figure 1; Figures A1 and A2). In addition, the dataset fills a major gap of soil radiocarbon measurements for sub-Saharan Africa by more than doubling the sampling density (Figure 1b). The dataset also increases the amount of data available outside of forested ecosystems, which are over-represented in most radiocarbon studies (Lawrence et al., 2020). Our analysis spans all main Köppen-Geiger climate zones (except deserts; Table S1) and soil types (Table S2) in sub-Saharan Africa, and includes disturbed (cultivated or eroded) and non-disturbed sites, enabling a unique comparison of SOC age and storage across and within a large variety of agro-ecological environments.

We focus on the relationship between SOC age and various soil and environmental properties (such as oxalate-extractable metals, crystalline minerals (1:1 and 2:1 clay minerals, pedogenic oxides), clay content, SOC content, climate zones, cultivation, erosion and gross primary productivity) in order to disentangle their different roles and importance in the SOC cycle. We concentrate on these variables because they can be represented by data available at broader scales, and their key role as important controls on SOC persistence has been previously demonstrated (i.e., Chen et al., 2021; Heckman et al., 2021; Khomu et al., 2017; Shi et al., 2020; Torn et al., 1997). We conclude our analyses with a discussion of regions where interactions between future climate and mineral SOC stabilization may alter the response of soils to climate change.

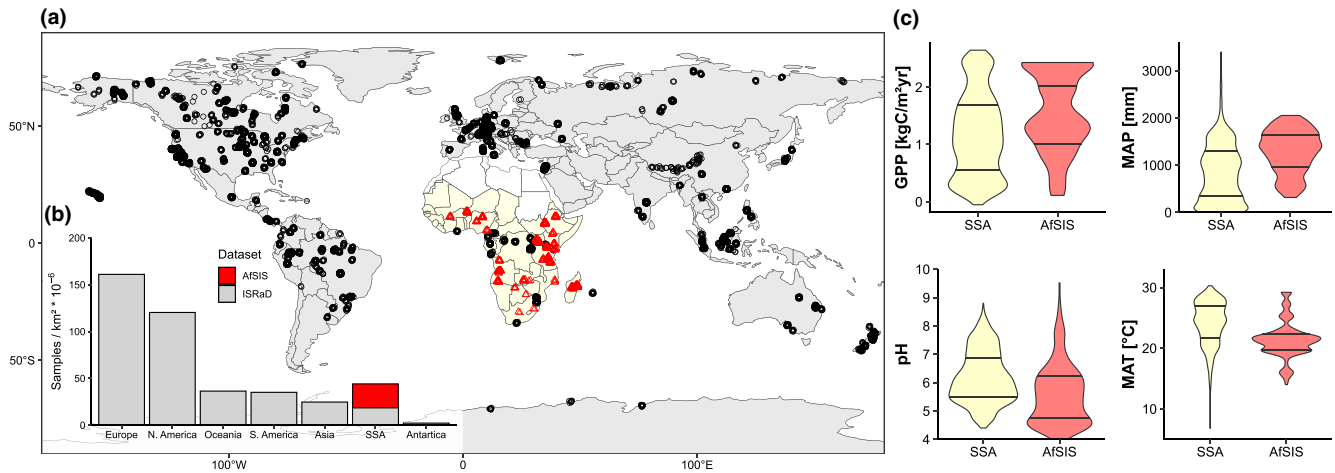


FIGURE 1 (a) Global map with all bulk $\Delta^{14}\text{C}$ soil samples (black circles) from the International Soil Radiocarbon Database (ISRaD 2.4.7.2023-02-01; $n_{\text{total}} = 6823$; $n_{\text{studies}} = 290$) and all $\Delta^{14}\text{C}$ soil samples (red triangles) from this study (AfsIS; $n_{\text{total}} = 510$); (b) Number of $\Delta^{14}\text{C}$ samples per $\text{km}^2 \times 10^{-6}$ for seven major land regions (Europe, North America, Oceania, South America, Asia, sub-Saharan Africa (SSA), Antarctica). Gray bars are based on data from ISRaD, red bar is based on data from this study; (c) violin plots for gross primary productivity (GPP), mean annual precipitation (MAP), pH and mean annual temperature (MAT) for sub-Saharan Africa (SSA; yellow) and this study (AfsIS; red). Horizontal lines indicate 25th and 75th quantiles, respectively. Map lines delineate study areas and do not necessarily depict accepted national boundaries.

2 | METHODS

2.1 | Sampling design

A total of 18,257 soil samples were collected from 60 sentinel sites (100 km²) and from two depth intervals (topsoil 0–20 cm and subsoil 20–50 cm) between 2010 and 2012 as part of the Africa Soil Information Service (AfsIS) project (Vågen et al., 2016). At each sampling location (1000 m²), samples from four sub-plots (100 m²) were combined into one sample. The sentinel sites are stratified across all major Köppen-Geiger climate zones that are present in sub-Saharan Africa (Figure 1a; Figure A1). The objective of the stratified random sampling design was to cover all major climate zones to avoid sample bias towards specific land covers (Lawrence et al., 2020) or soil types (Kögel-Knabner & Amelung, 2021). This sampling approach allows us to test whether findings based on a pre-defined transect with specific soil types (e.g., along a climate gradient for temperate forest soils) are comparable to results at a broader scale following a completely randomized sampling design.

For each plot, cultivated land, or being prepared for cultivation if sampling in the dry season, with annual or perennial crops and erosion (i.e., sheet, rill or gully/mass) were reported in the field. As a reference dataset, 2002 samples were selected for laboratory measurements (Vågen et al., 2021; von Fromm et al., 2021). The reference dataset was chosen to maximize the variation in the measured mid-infrared spectral data (Terhoeven-Urselmans et al., 2010). The selection strategy resulted in unequally distributed samples across 51 of the 60 sentinel sites, yet captured the variation in the original dataset (Tables S1 and S2; Figures S2–S4). For more details about the original sampling design and field survey, (see Vågen et al., 2013; von Fromm et al., 2021; Winowiecki, Vågen, Huisig, 2016; Winowiecki, Vågen, Massawe et al., 2016).

For this study, we selected only samples with complete and reliable data (no missing or negative values for any of the explanatory variables), with inorganic C < 0.1 wt-%, and for which archived profile samples (both topsoil and subsoil) were available. This reduced the number of samples to 514 out of the 2002 reference soil samples (von Fromm et al., 2023). The selected soil samples are from 30 sites from 14 countries across sub-Saharan Africa (Figure S1). We excluded all samples containing inorganic C because the removal of carbonates in these soils can leave residues of occluded inorganic C that provide more information on the dynamics of the inorganic C pools as opposed to organic C pools. Excluding samples with inorganic C ≥ 0.1 wt-% removed approximately 18% of the available samples. However, only 6% of the samples had inorganic C ≥ 1 wt-%, which is consistent with the land area of sub-Saharan Africa (4–5%) dominated by carbonate-rich soil types (Table S2). For a more detailed discussion about sampling density and data representativeness, see the supplementary material.

2.2 | Global data products

To investigate the effect of climate on the mean SOC age, we extracted the current (1980–2016) and future (2071–2100) Köppen-Geiger climate zones at 1 km resolution from Beck et al. (2018) for each soil profile ($n = 255$; Table 1 and Figure S1). The predicted climate zones are derived from an ensemble of 32 climate model projections based on the RCP8.5 scenario (see Beck et al., 2018). Gridded global data products usually come with large uncertainties, yet the Köppen-Geiger climate zones are a good approximation and integration of several climate parameters across sub-Saharan

TABLE 1 Grouping of the Köppen-Geiger climate zones based on absence/presence of dry season within each main Köppen-Geiger climate zone (capital letter) and summary statistics for extracted climate data at the profile level, including mean annual precipitation (MAP), potential evapotranspiration (PET), aridity index (PET/MAP; larger values refer to drier conditions), and mean annual temperature (MAT; median: minima-maxima).

New climate zone	Köppen-Geiger climate zone	MAP [mm]	PET [mm]	PET/MAP	MAT [°C]	n _{Profiles}
Arid	BWh (Arid, desert, hot)	542 (318–720)	2207 (1752–2937)	3.6 (2.6–7.2)	23 (18–29)	4
	BSh (Arid, steppe, hot)					35
	BSk (Arid, steppe, cold)					1
Temperate (seasonal)	Csb (Temperate, dry summer, warm summer)	1424 (776–1630)	1706 (1381–2164)	1.2 (1.0–2.8)	19 (14–22)	14
	Cwa (Temperate, dry winter, hot summer)					24
	Cwb (Temperate, dry winter, warm summer)					21
Temperate (humid)	Cfa (Temperate, no dry season, hot summer)	1725 (985–2054)	1445 (1413–1516)	0.8 (0.7–1.5)	20 (16–22)	76
	Cfb (Temperate, no dry season, warm summer)					1
Tropical (seasonal)	Aw (Tropical, savannah)	1349 (585–2011)	1759 (1389–2395)	1.3 (0.7–3.1)	22 (21–28)	48
Tropical (humid)	Af (Tropical, rainforest)	1184 (1156–1329)	1581 (1549–1676)	1.3 (1.2–1.4)	22 (22–23)	12
	Am (Tropical monsoon)					19

Abbreviations: MAP, mean annual precipitation; MAT, mean annual temperature; PET, potential evapotranspiration.

Africa. We used this grouping to examine differences between and within climate zones, as it is unlikely that a single soil property will explain SOC persistence across a wide range of climatic conditions (Rasmussen, Heckman, et al., 2018; von Fromm et al., 2021). In addition to the Köppen-Geiger climate zones, we extracted mean annual precipitation (MAP) and mean annual temperature (MAT; Fick & Hijmans, 2017), and potential evapotranspiration (PET; Zomer et al., 2022).

Based on the absence/presence of a dry season within each main Köppen-Geiger climate zone, we grouped the data into five groups: arid ($n_{\text{Profile}}=40$), temperate (seasonal; $n_{\text{Profile}}=59$), temperate (humid; $n_{\text{Profile}}=77$); tropical (seasonal; $n_{\text{Profile}}=48$); tropical (humid; $n_{\text{Profile}}=31$; Table 1). The newly formed climate groups contain data from at least eight different sites each, except for the temperate (humid) and tropical (humid) climate groups, which contain data from one and two different sites, respectively. However, the variation within these two climate groups are still well represented by our data, given the number of samples and the fact that a wide range of soil parameters were still represented within the gridded areas within each site (Figures S2–S4).

Gross primary productivity (GPP) was used as a rough proxy for plant C inputs. Data was derived from the FLUXCOM network (Jung et al., 2020) at a resolution of 0.0833° for each soil profile ($n=255$). FLUXCOM uses machine learning to merge carbon flux measurements from FLUXNET eddy covariance towers with Moderate Resolution Imaging Spectroradiometer (MODIS) satellite data (Jung et al., 2020). We averaged monthly values for the years 2001 to 2012.

2.3 | Laboratory measurements

A detailed description of all soil analyses conducted on the collected AFSIS reference database is provided by Vågen et al. (2021) and von Fromm et al. (2021). In brief, soil material was air-dried and sieved to a particle size <2 mm in the Soil-Plant Spectroscopy Laboratory at the World Agroforestry (ICRAF) in Nairobi, Kenya. All measurements used in this study were performed on the <2 mm fraction. Soil texture was determined by laser diffraction spectroscopy at ICRAF and the clay + fine silt fraction was defined as particles $<8 \mu\text{m}$. Particles $<8 \mu\text{m}$ include the most relevant particle sizes (clay + fine silt) to investigate the effects of mineral stabilization on SOC persistence. This approach is supported by previous work (von Fromm et al., 2021) which showed that particles $<8 \mu\text{m}$ resulted in a reproducible fraction across soil types based on duplicate measurements, in contrast to using only clay particles $<2 \mu\text{m}$. X-ray powder diffraction (XRPD) analysis was also performed at ICRAF and used for determining the amounts of crystalline mineral phases, including 2:1 and 1:1 clay minerals, pedogenic oxides and other minerals as detailed below. Soil organic (and inorganic) C content and oxalate-extractable metals (relevant to assess mineral C stabilization potentials) were determined at Rothamsted Research in Harpenden, UK. For all reference samples ($n=2002$), SOC was calculated from the difference between total C and inorganic C. The latter was measured by treating the sample with phosphoric acid and heating it to 135°C in a closed system. Inorganic C in the sample was converted to CO_2 and then measured by non-dispersive infrared detection

(NDIR). Total C was determined by combustion analysis. Poorly crystalline/amorphous minerals were quantified as the oxalate-extractable concentration of Al and Fe ($M_{ox} = Al_{ox} + Fe_{ox}$). Oxalate-extractable metals (M_{ox}) in wt-% were determined by extracting Al and Fe with oxalic acid and ammonium oxalate solution. The solution was shaken for 4 h at 25°C in the dark. Acid-oxalate extraction dissolves reactive minerals such as ferrihydrite (Fe), allophane and imogolite (Al), as well as other amorphous organic Fe and Al minerals (Parfitt & Childs, 1988). However, it may also attack non-target species, including maghemite and magnetite, and therefore releasing additional Al and Fe, as well as other organo-metal complexes (Reichenbach et al., 2023; Rennert, 2019). We interpret this extraction as a proxy for organo-mineral complex and amorphous mineral in general, rather than as a completely selective and fully quantitative method.

2.3.1 | Radiocarbon analysis

Radiocarbon (^{14}C) measurements were all performed in 2020 at the accelerator mass spectrometry facility of the Max-Planck Institute for Biogeochemistry, Jena, Germany (Steinhof, 2013) and measured on a mini carbon dating system (Micadas, IonPlus, Switzerland). Sample material was combusted in an elemental analyzer. The resulting CO_2 was reduced to graphite under the presence of H_2 , with iron as a catalyst (Steinhof et al., 2017). On-line $\delta^{13}\text{C}$ measurements at the combustion stage revealed that two samples out of the 514 samples used for this study contained significant amounts of carbonates ($\delta^{13}\text{C} = -6.2$ and -4.5%). The corresponding profiles were removed from the final analyses, resulting in a total of 510 soil samples. Samples with low organic C content (<0.3 wt-%; $n=32$) were measured using the gas inlet system of the Micadas, resulting in lower precision ($5.4 \pm 0.3\%$) compared to those measured as graphite ($2.2 \pm 0.5\%$).

We report ^{14}C data as $\Delta^{14}\text{C}$, which is corrected for the decay of the oxalic acid standard between 1950 and the measurement year 2020. In order to account for mass-dependent fractionation effects, the $^{14}\text{C} / ^{12}\text{C}$ ratio of all samples is corrected to a common $\delta^{13}\text{C}$ value of -25% (Stuiver & Polach, 1977). The measured $\Delta^{14}\text{C}$ values were used to estimate the mean SOC age in each soil sample. This was done by applying a one-pool model that includes the uptake of 'bomb' ^{14}C added to the atmosphere by nuclear weapons testing between ca. 1950 and 1964. The model provides a relative measure of C dynamics and assumes that SOC is homogenous and at steady-state (Shi et al., 2020; Trumbore, 2009). The calculations were performed using the R package *SoilR* (Sierra et al., 2014; R code can be found on *github*) following the approach by Torn et al. (2009).

In cases where two mean SOC ages yielded the same $\Delta^{14}\text{C}$ value (i.e., in cases where $\Delta^{14}\text{C} > 0\%$), we report only the older mean SOC age, as it is more consistent with the fluxes of C into and out of the mineral associated and bulk soil fractions (Gaudinski et al., 2000; Shi et al., 2020). While this approach is highly simplified, given that

measurements of bulk soil represent a mixture of older and younger SOC, the estimated mean SOC ages still provide a useful indicator for how much time has passed on average since the C was fixed from the atmosphere. Under the presented model assumptions, mean SOC age is equal to the turnover rate (Khomu et al., 2017; Shi et al., 2020; Trumbore, 2009). Modeling approaches have shown that SOC age distributions have a long tail of old C, suggesting that a small fraction of SOC persists in soils much longer compared to the majority of SOC; mean SOC ages may thus underestimate the rate of response of SOC to changes in vegetation inputs or climate (Sierra et al., 2018).

2.3.2 | Crystalline mineral quantification

Concentrations of crystalline minerals were quantified through X-ray powder diffraction (XRPD). Sample preparation and data collection were carried out using the procedure outlined in Butler et al. (2020). Briefly, subsampled and milled soils were loaded onto a Bruker D2 PHASER diffractometer equipped with a Cu-K α radiation source and Ni-filter. Quantification of crystalline minerals from the XRPD data was achieved using the automated full pattern summation (*afps*) function implemented in the *powdR* package v1.3.0 for R (Butler & Hillier, 2021b). The observed diffractograms were modeled as the sum of scaled pure patterns provided by open-source libraries that are included with *powdR* (Butler & Hillier, 2021b; Eberl, 2003). A total of 108 reference patterns from these open-source libraries were supplied to the *afps* function, which together accounted for all major and minor soil components detectable within the AfSIS dataset. The *afps* function first selects the appropriate reference patterns from the full set to use for each sample, before scaling them by an optimization routine to minimize an objective function that summarizes how well the fitted and observed patterns matched (full details provided in Butler & Hillier, 2021a, 2021b). The optimized scaling coefficients are then combined with Reference Intensity Ratios (RIRs), a measure of each phase's diffracting power that are also provided within the *powdR* reference libraries. Mineral quantifications are expressed in units of weight-% of the crystalline mineral component of the sample.

The limits of detection (LOD) for all phases identified from the XRPD data were estimated using the RIRs and the method described in Butler and Hillier (2021a). Different phases diffract X-rays with different power (reflected in the RIRs) and, hence, have different LOD. For example, a strong diffractor such as quartz, with a RIR of 5.8, would have a smaller LOD than a weak diffractor such as kaolinite (RIR~0.5). The LOD of the internal standard quartz (RIR=5.8) was assumed to be 0.1%, from which the LOD of each other phase can be estimated using its RIR:

$$\text{LOD} = 0.1 \times (5.8 / \text{RIR})$$

Based on the above equation, K-feldspar phases (RIR~1), for example, have an estimated LOD of 0.6%, and kaolinite phases (RIR~0.5) have an estimated LOD of 1.2%.

For quality control, all resulting fits derived from the *afps* function were manually inspected. The agreement between the fitted and observed patterns was satisfactory for each fit, aligning with that found when the same approach was tested on challenging clay-bearing mixtures from interlaboratory tests (Butler & Hillier, 2021a).

It is important to note that we did not have XRPD data available for every radiocarbon sample. This is because the XRPD data is from a different subset of the AfSIS datasets than the radiocarbon samples. In total, we have 318 unique XRPD samples, of which 164 samples also have radiocarbon values. For the remaining radiocarbon samples, we always used an XRPD sample that is from the same cluster (1 km²) as the radiocarbon sample. The average distance between a radiocarbon sample and the corresponding XRPD sample is 540 m and the maximum distance is 1059 m. Since there are sometimes multiple radiocarbon samples within the same cluster, there are some XRPD samples that were used for more than one radiocarbon sample. We performed a preliminary analysis using only soils with exactly paired XRPD and $\Delta^{14}\text{C}$ data. The results were in accord with those obtained by examining the entire dataset.

Finally, to derive common soil mineral groups, we used the following mineral concentrations from the quantitative analysis:

Feldspars = K-feldspar + Plagioclase
 Quartz = Quartz
 2:1 clay minerals = Smectite (ML and Di) + Illite + Vermiculite
 1:1 clay minerals = Kaolinite + Dickite + Halloysite
 Pedogenic oxides = Goethite + Maghemite + Hematite + Magnetite + Gibbsite
 Other = all other minerals quantified (see [Supporting Information data](#))

We used this mineral grouping, because they reflect different weathering conditions, chemical and physical characteristics

relevant for SOC dynamics (Table 2). For example, previous work from sub-Saharan Africa has shown that poorly crystalline minerals and 2:1 clay minerals are generally associated with older ¹⁴C ages, while 1:1 clay minerals and pedogenic oxides are associated with younger ¹⁴C ages (Khomu et al., 2017; Wattel-Koekkoek et al., 2003). Feldspars are rock-forming primary minerals that are easily weatherable (Wilson, 1975), whereas quartz is an inert primary mineral (Polynov et al., 1937).

2.4 | Statistical analyses

Principal component analysis (PCA) was performed for the two depth layers (topsoil: 0–20 cm; subsoil: 20–50 cm) to visualize and further explore the relationship between SOC persistence, climate, mineralogy, and land degradation (caused by cultivation and/or erosion). Clay + fine silt fraction (<8 μm), 1:1 and 2:1 clay mineral content, poorly crystalline minerals (M_{ox}), pedogenic oxides, feldspars, quartz, and gross primary productivity were used to calculate the principal components to capture different controls on SOC persistence. Mean SOC age and content, climate zones, land cover, and erosion were used as supplementary variables for the PCA. This was done to test how well these variables are described by the other variables (Lê et al., 2008). One-way anovas were performed to test which of the categorical variables best describe the distance between individuals. The PCA coordinates of the supplementary variables are predicted using only the information provided by the performed component analysis on the other variables and all individuals. All numerical variables were normalized and scaled prior to conducting the PCA.

We used linear mixed-effects models as a quantitative tool to account for the hierarchical and nested sampling design of the AfSIS dataset (clusters within sites and two sampling depths within

TABLE 2 Median ± median absolute deviation (in wt-%) of the main mineral groups, including feldspars, poorly crystalline mineral, 2:1 clay mineral, 1:1 clay mineral, pedogenic oxides and quartz concentrations across climate zones for topsoils (0–20 cm) and subsoils (20–50 cm), respectively.

Climate zones	Depth	Feldspars	Poorly crystalline	2:1 clay minerals	1:1 clay minerals	Pedogenic oxides	Quartz
Arid	Topsoil	3.5 ± 5.2	0.1 ± 0.1	2.2 ± 3.2	2.5 ± 3.6	2.9 ± 4.3	72.6 ± 30.0
	Subsoil	2.7 ± 4.1	0.2 ± 0.1	1.7 ± 2.5	4.7 ± 6.9	3.8 ± 5.6	70.9 ± 30.0
Temperate (seasonal)	Topsoil	12.6 ± 13.0	0.6 ± 0.5	6.6 ± 9.8	12.8 ± 15.3	7.9 ± 8.8	23.7 ± 31.4
	Subsoil	11.8 ± 10.5	0.5 ± 0.4	8.4 ± 9.2	13.3 ± 13.1	8.8 ± 9.1	18.4 ± 23.4
Tropical (seasonal)	Topsoil	13.9 ± 15.6	0.3 ± 0.2	2.0 ± 3.0	7.2 ± 4.6	5.1 ± 3.2	53.7 ± 39.4
	Subsoil	14.3 ± 15.7	0.3 ± 0.2	2.6 ± 3.9	11.3 ± 6.6	5.0 ± 2.5	48.9 ± 36.3
Temperate (humid)	Topsoil	<LOD	0.7 ± 0.2	<LOD	22.7 ± 9.2	24.2 ± 14.5	29.3 ± 16.8
	Subsoil	<LOD	0.6 ± 0.2	<LOD	22.5 ± 12.0	24.2 ± 14.9	29.7 ± 16.4
Tropical (humid)	Topsoil	2.1 ± 0.9	0.5 ± 0.3	2.8 ± 1.6	14.1 ± 8.2	5.1 ± 3.3	57.1 ± 7.8
	Subsoil	2.0 ± 1.0	0.4 ± 0.2	2.8 ± 4.1	14.8 ± 8.6	8.9 ± 6.0	49.7 ± 14.1

Note: All crystalline minerals are derived from the XRPD data and poorly crystalline minerals are the sum of oxalate-extractable metals ($M_{ox} = Al_{ox} + Fe_{ox}$). Together with the remaining minerals (not shown) all the crystalline minerals add up to 100 wt-%.

Abbreviation: LOD, below limit of detection.

each profile; von Fromm et al., 2021). The variance inflation factor was used to check for multicollinearity among predictor variables with a threshold of <3.0 (Zuur et al., 2010). To meet linear mixed-effects assumptions and to standardize variation among variables, all continuous parameters were transformed and standardized to a normal distribution using Box-Cox transformation (Peterson & Cavanaugh, 2020). We started from a constant null model with siteID/clusterID/plotID as random effects and then extended the model stepwise by fitting the following sequence of fixed effects: MAP, MAT, depth, cultivation, erosion, GPP, SOC, 2:1 clay minerals, M_{ox} , 1:1 clay minerals, pedogenic oxides, clay + fine silt content, quartz, and feldspars. The order of fixed effects was predefined based on a priori knowledge and their hypothesized importance in explaining variation in SOC age across sub-Saharan Africa, starting with large-scale climate variables and ending with fine-scale physicochemical soil properties (Burnham & Anderson, 2002). The maximum likelihood method and likelihood ratio tests (L.ratio) were applied to evaluate model performance and the statistical significance of the added fixed effects (Tables S4–S6). The variation of SOC age explained by each fixed effect was obtained by calculating the marginal R^2 (excluding the variation explained by the random effects) for each model and subtracting the R^2 from the previous fitted model (Nakagawa & Schielzeth, 2013). To identify differences in the controls on SOC age with depth and across climate zones, we built multiple models: for all samples; topsoil only; subsoil only; and a model for each climate zone (without including depth, MAT and MAP as fixed effects and including topsoil and subsoil samples together). We did not include depth as a predictor in the climate models because SOC age is known to be strongly correlated with depth (e.g., Shi et al., 2020), and the topsoil and subsoil only models showed similar controls (Figure S5). For the climate zone models, we were primarily interested in identifying similarities and differences in the controls of the other explanatory variables.

A random forest model was used to identify nonlinear relationships between SOC age and any explanatory variable, as well as to identify differences across pedo-climatic zones. We built a model with the same explanatory variables as for the climate zone explicit linear-mixed effects models, except we did not include erosion and cultivation as predictors. This is because we are mainly interested in identifying and understanding differences in physicochemical controls across climate zones. For the validation of the resulting regression model, we performed a 10-fold cross validation, ensuring that soil profiles from the same cluster within a particular site were either in the training or testing dataset. Model evaluation was performed on the testing dataset, including the calculation of R^2 and the mean absolute error (MAE). To better interpret the outcome of the random forest model, we used partial dependence plots and individual conditional expectation plots. The partial dependence plots show the marginal effects an explanatory variable has on the predicted outcome of the random forest model while holding all the other variables constant that have been used to build the random forest model (Friedman, 2001). Individual conditional expectation plots are similar to partial dependence plots, but instead show one line

per observation that shows how the prediction of an observation changes when the value of an explanatory variable for that observation changes (Goldstein et al., 2015; Molnar, 2022). Rather than plotting a prediction line for each observation, we calculated the median of subsets of observations based on their climate zones. This allows us to interpret the importance of each explanatory variable in these zones, respectively. Vertical lines next to each panel show the range of predicted mean SOC age for one explanatory variable, while holding all other variables constant. Note that we did not use the random forest model to do any upscaling. Instead, we used it to better understand the nonlinear behavior between SOC age and the explanatory variables and how their relationship may differ across climate zones. Predictions outside the data range of the majority of samples should be interpreted with caution.

All statistical analyses were performed within the R computing environment (version 4.1.1; R Core Team, 2021) including the additional R packages *ggpubr* (Kassambara, 2020), *tidyverse* (Wickham et al., 2019), *tmap* (Tennekes, 2018), *raster* (Hijmans, 2021), *scales* (Wickham & Seidel, 2022), *sf* (Pebesma, 2018), *FactoMineR* (Lê et al., 2008), *factoextra* (Kassambara & Mundt, 2020), *mlr3* (Lang et al., 2019), *iml* (Molnar et al., 2018) and *nlme* (Pinheiro et al., 2020).

3 | RESULTS

The climate grouping largely reflects different pedo-climatic conditions across sub-Saharan Africa (Tables 1 and 2). At this broad scale, the climate zones integrate many soil forming factors and can be seen as a conservative grouping of soil profiles that may locally be highly diverse, yet are confronted with a similar set of underlying broad scale environmental factors. Arid soils have the highest concentration in quartz minerals (Table 2) and are characterized by limited chemical weathering due to water-limitation and low plant biomass production. Quartz is a mostly inert mineral with negligible contributions to total and extractable soil nutrients (Butler et al., 2020; Hardy & Cornu, 2006). In contrast, soils under seasonal climate (temperate and tropical) show relatively high concentration in feldspars and 2:1 clay minerals (Table 2), reflecting their intermediate weathering status (Jackson et al., 1948). Lastly, highly weathered soils from humid regions (temperate and tropical) are characterized more by 1:1 clay minerals and pedogenic oxides (Feller & Beare, 1997; Ojanuga, 1979).

Across sub-Saharan Africa, we found relatively young mean SOC ages, which is in contrast to the long development times for most of these soils (several hundred thousand years; Jones et al., 2013). Averaged over all sampling locations, mean SOC ages are 182 ± 62 years (median \pm median absolute deviation) in topsoils (0–20 cm) and 563 ± 227 years in subsoils (20–50 cm; Figure S6). For the topsoil samples, mean SOC age decreases with increasing SOC content, with a threshold at about 1 wt-% SOC content. Samples with a SOC content >1 wt-% usually do not show mean SOC ages below 500 years, whereas samples with a SOC content <1 wt-% can

have older mean SOC ages (Figure 2a), reflecting faster turnover rates at higher SOC content. We found the same overall patterns for subsoils (Figure S7b), and will only focus on topsoils in the main part of the manuscript (see Figures S5–S8, S11, S12 for more detailed analysis of subsoils).

The youngest mean SOC ages are in highly weathered soils in humid climate zones (topsoil: 140 ± 46 years; subsoil: 454 ± 247 years; Figure 2a), whereas the oldest SOC ages are found in soils of arid climate zones (topsoil: 396 ± 339 years; subsoil: 963 ± 669 years). Seasonal climate zones show a higher variation in mean SOC age (topsoil: 201 ± 130 years; subsoil: 645 ± 385 years) compared to humid soils (Figures 2a and 3b).

The principal component analysis (PCA) for the topsoils shows that climate zones significantly correlate with variables that control both SOC content (dimension 1: $R^2=0.57$, p -value <0.001) and SOC age (dimension 2: $R^2=0.29$, p -value <0.001 ; Figure 2b). Mean SOC age positively correlates with dimension 2 (correlation coefficient = 0.29, p -value <0.001), whereas SOC content positively correlates with dimension 1 (correlation coefficient = 0.73; p -value <0.001). In the positive direction of dimension 2, concentrations in 2:1 clay minerals (correlation coefficient = 0.92), feldspars (correlation coefficient = 0.81), and poorly crystalline minerals (correlation coefficient = 0.33) are most correlated. In contrast, humid soils are characterized by high concentrations of 1:1 clay minerals, pedogenic oxides and GPP, which all show a negative correlation with mean SOC age and a positive correlation with dimension 1, respectively. The same patterns occur for the subsoil samples (Figure S7b). Overall, the PCA confirms that climate grouping at this broad scale includes soils with relatively distinct pedo-climatic conditions that permit further exploration of the relationship between soil mineralogy and mean SOC ages across and within these pedo-climatic groups.

The linear-mixed effects model for all samples explains 66% of the variation in SOC age across sub-Saharan Africa. Climate variables (MAT and MAP) add less than 10% to the total explained variation.

About half of the variation is explained by depth (32%), followed by C inputs (GPP: 8% and SOC content: 3%), and mineral controls (M_{ox} : 5% and clay + fine silt content: 3%). The linear-mixed effects models further show that controls between topsoil and subsoil samples are similar, yet climate and GPP are slightly more important in topsoil samples, whereas mineral controls are more important in subsoils (Figure S5 and Table S3). Soils from seasonal climate zones with more high-activity clays and poorly crystalline minerals (Table 2) have a wider range and include older SOC ages compared to soils from humid climate zones (Figure 3b). In particular, M_{ox} and 2:1 clay minerals explain the highest variation in SOC age in seasonal climate zones (ca. 20%) across all climate zones (Figure 3a). As weathering progresses, SOC stabilizing minerals (2:1 clay minerals and poorly crystalline minerals) will weather to 1:1 clay minerals and other crystalline minerals prevalent in humid climate zones, resulting in younger SOC ages. The presence of poorly crystalline minerals in humid soils does not explain much of the variation in SOC age (ca. 4%; Figure 3a). Soils from humid regions are characterized by the highest and narrowest GPP values (Figure 3b). However, the variation in SOC age in humid regions (temperate and tropical) is predominantly explained by SOC content (62%; Figure 3a). Across all climate zones, GPP is most important in arid regions (21%; Figure 3a).

The random forest model for all samples explains about 46% of the variation in SOC age across sub-Saharan Africa, with a mean absolute error of 263 years (Figure S9). Across all climate zones, higher concentrations of 2:1 clay minerals and oxalate-extractable metals always result in older predicted SOC ages, whereas 1:1 clay minerals have no effect on the predicted SOC ages (Figure 4b,c). For 2:1 clay minerals and oxalate-extractable metals, there are some thresholds evident, however most of them fall outside the 75th percentile data range (as indicated by the boxplots) and should be interpreted with caution (Figure 4b,d). Although the clay + fine silt fraction significantly explains variation in SOC ages in each climate zone (Figure 3a; Table S3), it only results in older SOC ages at values $>75\%$ based on the random forest model (Figure 4a). For all mineral predictors,

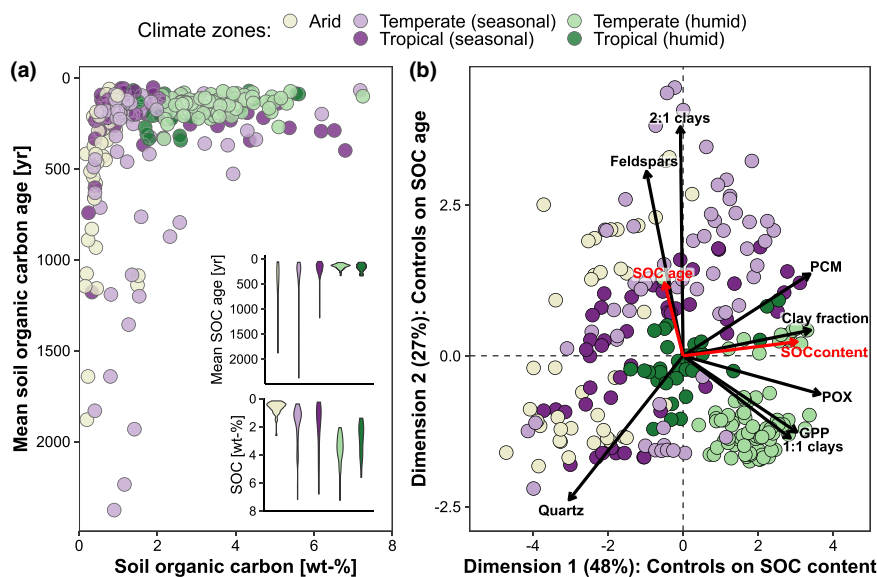


FIGURE 2 (a) Mean soil organic carbon (SOC) age and SOC content colored by climate zones. Insets show violin plots for mean SOC age and SOC content. Note that y-axes show different scales. (b) Principal component biplot for dimension 1 and 2 colored by climate zones. Mean SOC age and content (red arrows) were not used to derive the principal components. Only topsoils (0–20 cm) are shown for both plots. Subsoils showed similar patterns (see Supporting Information, Figure A7). GPP, gross primary productivity; PCM, poorly crystalline minerals; POX, pedogenic oxides.

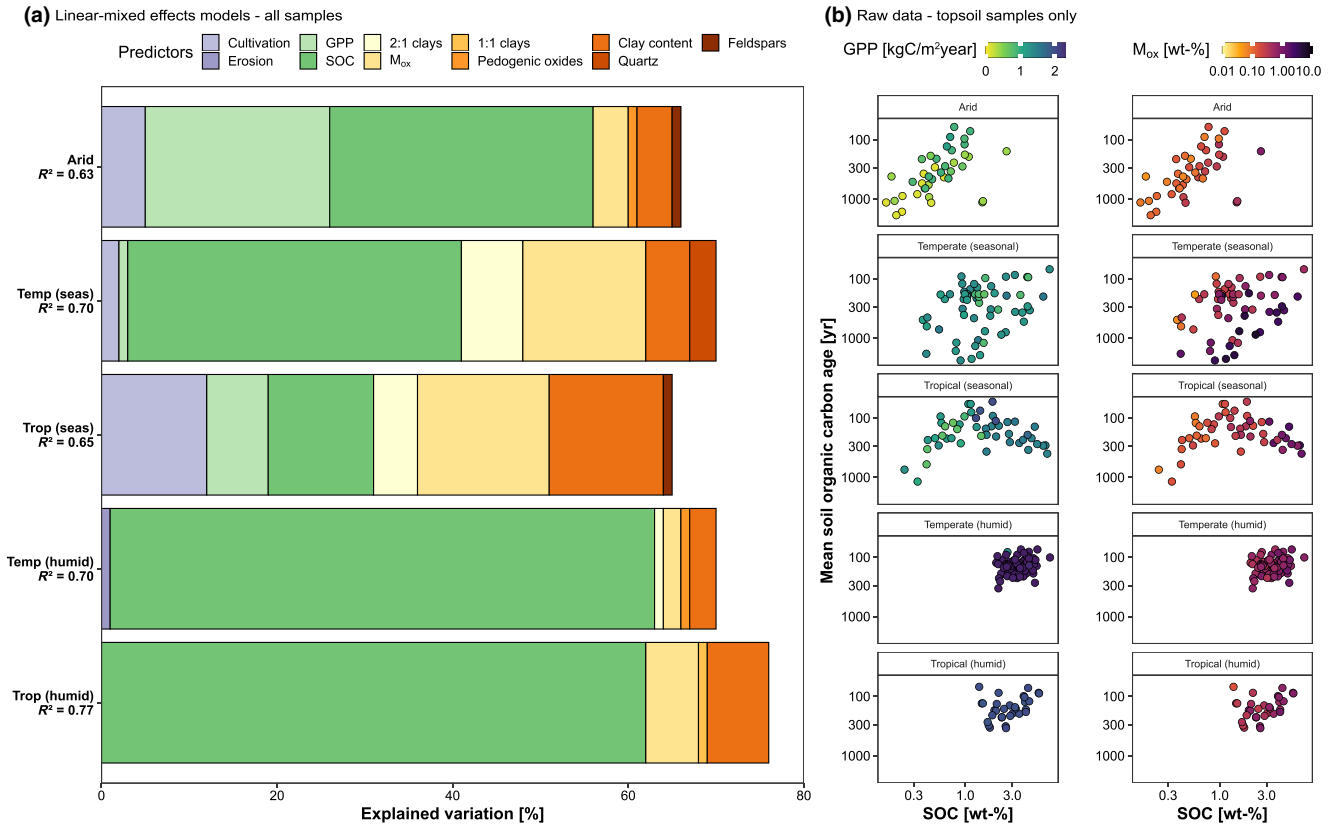


FIGURE 3 (a) Explained variation of SOC age (based on marginal R^2) for each fixed effect, based on sequential fitting of the linear mixed-effects models for each climate zone, respectively. (b) Mean soil organic carbon (SOC) age (log-scaled) and SOC content (log-scaled), colored by gross primary productivity (GPP) and oxalate-extractable metals ($Al_{ox} + Fe_{ox}$; log-scaled) for topsoil only (0–20 cm). Subsoils show similar patterns, see [Figure S8](#).

except for 1:1 clay minerals, the differences in the predicted SOC ages are largest in seasonal and arid climate zones (as indicated by the horizontal lines; [Figure 4](#)).

In terms of the effects of land degradation on SOC persistence, cultivated or eroded soils have on average older mean SOC ages and show a greater variability in mean SOC ages compared to non-disturbed soils ([Figure S10](#)). However, neither our PCA analysis nor the linear mixed-effects models identified cultivation or erosion as important variables at this broad scale ([Table S3](#), [Figures S5](#), [S11](#) and [S12](#)), except in tropical (seasonal) climates ([Figure 3a](#)). This is also reflected in the raw data for sites where cultivated/eroded plots are in close proximity to non-cultivated/non-eroded plots and do not show a clear pattern ([Figure S10](#)).

4 | DISCUSSION

Relationships between mineralogy, climate, vegetation productivity, and soil carbon age found at the local scale hold at the continental scale—something that has not previously been demonstrated for the wide variety of soil types found in sub-Saharan Africa. We use climate zones to group soils with respect to SOC content and age, resulting in distinct pedo-climatic regions across sub-Saharan Africa.

This approach allows us to sort and structure diverse landscapes according to underlying mechanisms that explain SOC persistence at broader scales ([Figure 5](#)). For example, mean SOC ages from arid and humid climate zones are driven by bio-climate factors, including GPP and SOC content, whereas reactive minerals are most important in explaining variation in mean SOC ages in seasonal climate zones ([Figures 3](#) and [4](#)). The composition and complexity of the factors operating in the different pedo-climatic regions highlights the need to incorporate a process-oriented representation of soils in models that aim to represent C cycling at broader scales, rather than trying to identify a single soil or climate property that best describes SOC persistence ([Jungkunst et al., 2022](#)). Our improved understanding also contributes to more process-oriented future projections of soils under climate change. In the following section, we will discuss the underlying mechanisms for SOC persistence across the identified pedo-climatic regions and how these different regions may respond to climate change.

4.1 | Humid climate zones

In more humid climate zones (without a pronounced dry season), higher mean annual precipitation and a more even distribution of

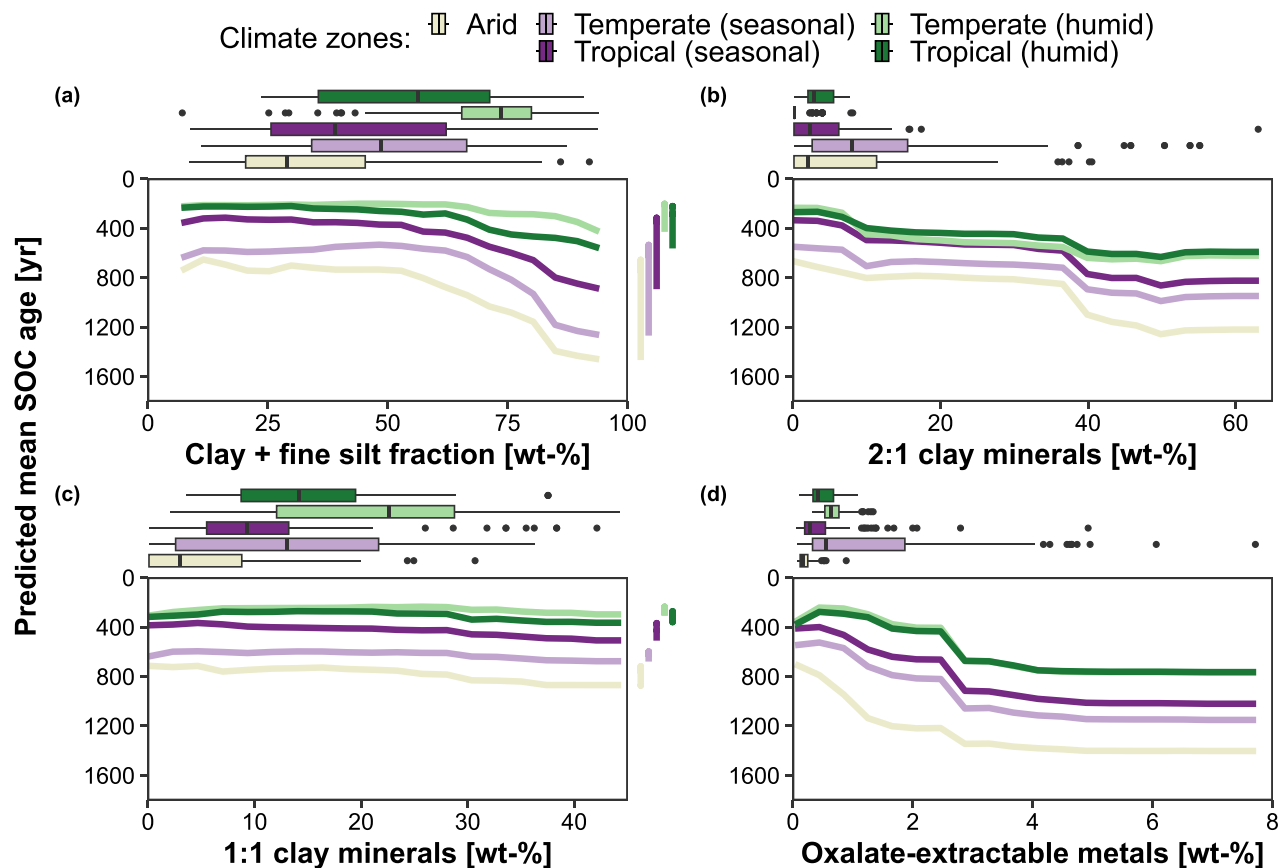


FIGURE 4 Individual conditional expectation plots derived from the random forest model grouped by climate zones. Boxplots above each panel show the raw data distribution for each explanatory variable, and vertical lines next to each panel show the range of the predicted mean soil organic carbon (SOC) ages for each climate zone over the range of one explanatory variable, while holding the other variables constant. Figure shows results for (a) clay + fine silt content, (b) 2:1 clay minerals, (c) 1:1 clay minerals, and (d) oxalate-extractable metals.

rainfall allows for a longer growing season and results in higher GPP (Figure 3b), greater soil C inputs and more rapid decomposition of SOC. However, since these soils have relatively high concentration in 1:1 clay minerals with limited capacity to stabilize SOC, higher C input will not necessarily lead to higher SOC concentrations (Table 2; Figures 2b and 5; Khomo et al., 2017; Six, Feller, et al., 2002; Wattel-Koekkoek et al., 2003). The potential of deeply weathered soils that dominate these regions is often limited in its capacity to stabilize C inputs (Georgiou et al., 2022; Reichenbach et al., 2023), while microbial decomposition is high (Cusack et al., 2009). Our findings thus support the idea that some of the geochemically older tropical soils in humid climate zones may be closer to SOC 'saturation' (Six, Conant, et al., 2002). Therefore, deeply weathered tropical soils likely have a low potential for long-term sequestration of SOC, even if C inputs increased in the future (Reichenbach et al., 2023; Sayer et al., 2019).

Interestingly, the presence of poorly crystalline minerals does not necessarily result in older SOC ages in soils under humid climates compared to seasonal climates (Table S3 and Figure 3). Although many studies have reported a positive relationship between oxalate-extractable metals and SOC persistence (Chen et al., 2021; Masiello et al., 2004; Rasmussen, Throckmorton, et al., 2018; Torn et al., 1997), others have found no consistent pattern (Hall et al., 2018; Heckman

et al., 2021). While tropical soils are often rich in pedogenic oxides (e.g., gibbsite and goethite) especially at advanced weathering stages, most of it is also locked away in stable Fe/Al concretions that do not readily interact with new C inputs as is known for temperate soils during aggregate formation (Martinez & Souza, 2020). However, for those mineral surfaces that come in contact with the soil solution, it is known that Fe-bearing minerals are sensitive to moisture changes and therefore constantly adsorb and release SOC from their mineral surfaces (Chen et al., 2020; Thompson et al., 2011). Similarly, the stability of sorption strength of minerals can be affected by local changes in pH near the rhizosphere (Keiluweit et al., 2015). As a result, cyclic fluctuations in moisture, acidity and O_2 levels affect the solubility of Fe and can release sorbed organic matter for decomposition by microbes (Hall & Silver, 2013; Song et al., 2022). Therefore, these fluctuations with frequent rainfall, together with continuous high plant C inputs and decomposition, are likely to keep SOC ages young and overall highly dynamic in soils of humid climate zones across sub-Saharan Africa. In addition, it could also be that poorly crystalline minerals reflect greater intensity of mineral weathering by organic acids and are therefore driven by higher C inputs in these soils (Hall & Thompson, 2022). Ultimately, at this large scale, we cannot disentangle these mechanisms entirely.

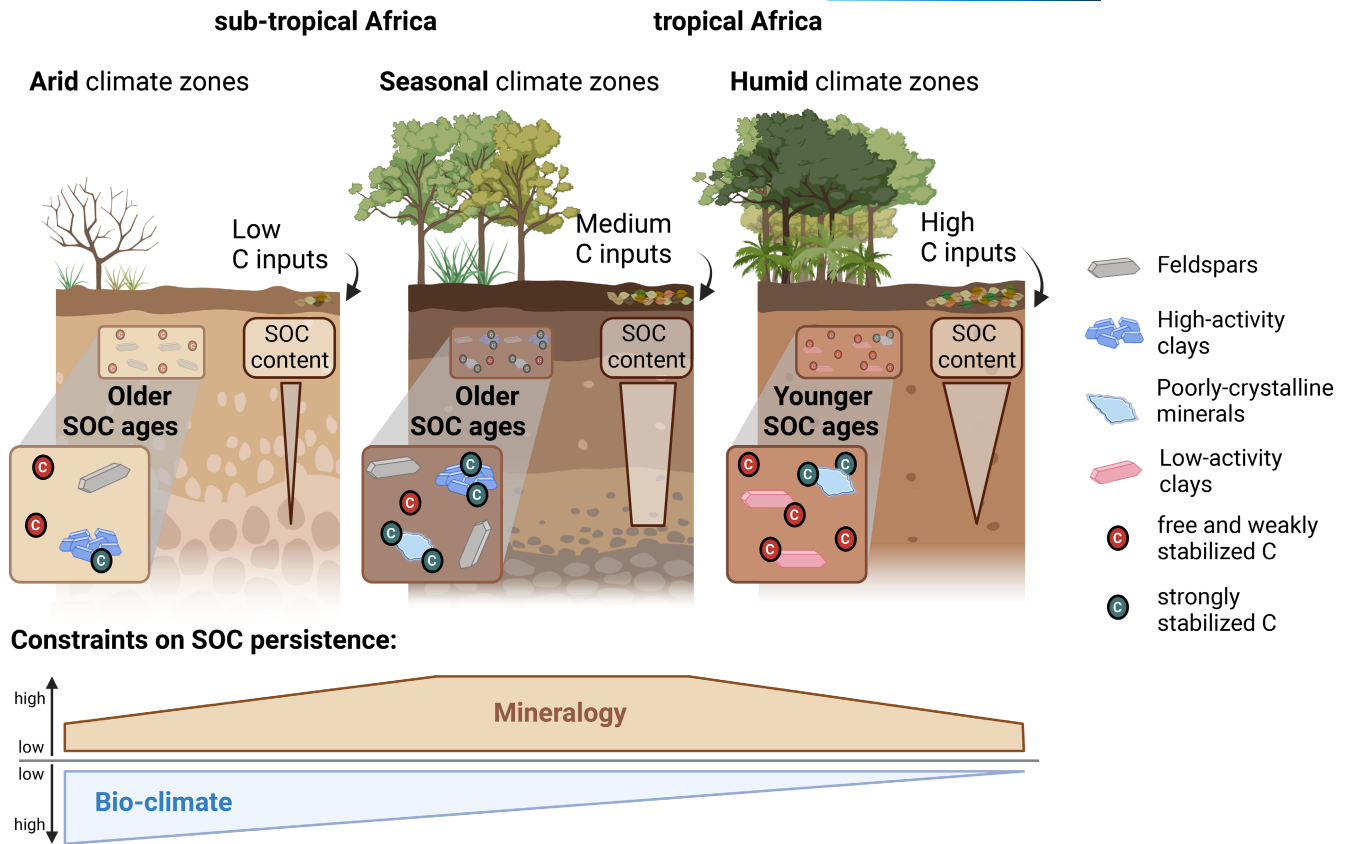


FIGURE 5 Schematic figure of bio-climate and mineral controls on soil organic carbon stabilization across sub-Saharan Africa. Feldspars: K-feldspars and Plagioclase; High-activity clays: 2:1 clay minerals such as smectite and vermiculite; poorly crystalline minerals: oxalate-extractable metals ($Al_{ox} + Fe_{ox}$); low-activity clays: 1:1 clay minerals (kaolinite) and pedogenic oxides (e.g., Goethite, Gibbsite and Hematite). The figure was created with biorender.com.

4.2 | Seasonal climate zones

In seasonal climate zones, the direct importance of climate for SOC age tends to be smaller, as indicated by the larger distance between individual observations in the PCA compared to the other climate zones (Figure 2b) and the on average smaller importance of SOC content and GPP (Figure 3a). Interestingly, variation in GPP is not directly related to younger SOC ages and only partly to higher SOC content (Figure 3b). Thus, soils in seasonal climate zones might be less responsive to alteration in GPP caused by future climatic changes, than their counterparts in arid and humid climate zones.

Soils in seasonal climates are characterized by higher concentrations of high-activity clays (2:1 clays) and poorly crystalline minerals, which provide excellent conditions for C sorption, resulting in older SOC ages compared to soils from humid climate zones (Figures 3 and 4). The observed older SOC ages with the presence of reactive minerals is in agreement with the understanding that organo-mineral interactions associated with poorly crystalline minerals and/or 2:1 clay minerals create physico-chemical barriers that restrict microorganisms from decomposing organic molecules (Khomu et al., 2017; Six, Feller, et al., 2002; Wattel-Koekkoek et al., 2003), leading to high amounts of mineral protected SOC. Thus, as the variation in climate (limiting or promoting weathering and plant C input) and

mineral properties (derived from parent material and the stage of soil development) are the most diverse, soils in seasonal climate zones have the widest range of SOC content and age combination of all sub-Saharan Africa regions studied (Figures 2a, 3 and 4). Our findings that mineral reactivity is as important as C input in representing SOC persistence, and more important than the amount of clay + fine silt fraction in these regions (Figures 3 and 4) also have implications for global-scale approaches. Most global-scale studies attempt to model C cycling often without precise data to represent the soil mineral phase (Shi et al., 2020; Tifafi et al., 2018). However, describing the reactive inorganic component of soil as a single numeric value based on particle size alone overlooks the intricate influence of multiple reactive components that can exist within this size range (Butler et al., 2020; Feller & Beare, 1997; Hassink, 1997; Six, Conant, et al., 2002).

4.3 | Arid climate zones

Arid soils have the oldest SOC ages even though reactive minerals are less abundant than in seasonal climates (Figures 3 and 4). We explain this finding by the strong climatic barriers that exist in this zone for biological processes due to low moisture availability for most of

these soils (Table 1). This results in both low plant C inputs (low GPP; Figures 2b and 3b) and limited microbial C decomposition. However, Quéro et al. (2022) showed for plowed Arenosols that the remaining SOC was of microbial origin and stabilized within organo-mineral associations. Similarly, Khomo et al. (2017) found for arid soils in South Africa that some SOC was associated with Fe(oxhydr)oxides. In arid soils, these minerals can be very stable (i.e., not much fluctuation in oxide stability) and thus they could stabilize SOC for longer time than in humid soils with fluctuating redox potential (Bhattacharyya et al., 2018). This is reflected in our linear mixed-effects model for arid samples and the random forest model, where a higher concentration in poorly crystalline minerals results in older SOC ages (Table S3; Figure 4d), although the explained variation is only 4% (based on the linear mixed-effects model; Figure 3a). Photo-oxidation of fresh and young SOC may also contribute to overall older mean SOC ages in these arid regions (Austin & Vivanco, 2006), as may the deposition of aeolian dust and the presence of charcoal, both of which can contain relatively old C (Cusack et al., 2012; Eglinton et al., 2002). In summary, old SOC ages in the arid zone appear to be more a function of constraints on weathering, C inputs, and C mineralization (Figure 3). Small increases in precipitation may promote C stabilization of inputs if reactive minerals are already present (for example, formed in a wetter past climate; Figure 4b,c).

4.4 | Anthropogenic factors

Our data show that anthropogenic disturbances are detectable in mean SOC age at broader scales (Figure 3a), yet the direction and magnitude remain uncertain (Table S3 and Figure A10). For eroded soils, the older mean SOC ages are likely due to the removal of younger SOC from the topsoil layer (Berhe et al., 2008; Paul et al., 1997), whereas for cultivated soils, lower C inputs of fresh (young) C could result in older mean SOC ages (Harrison et al., 1993; Wang et al., 1999). However, when comparing eroded/cultivated vs. non-eroded/non-cultivated soils from the same site, they show different responses with respect to SOC ages, which could be for various reasons. For example, it has been shown that different management practices can have varying effects on SOC dynamics (Six, Feller, et al., 2002; Winowiecki et al., 2016). In addition, cultivation is typically performed on fertile soils, that are, as identified above, associated with a particular climate and mineralogy (Figure 3a). Furthermore, cultivation may also increase the risk of erosion if it takes place in regions that are topographically and climatically prone to promote soil redistribution (Lal, 1985). All of this suggests that the effect of cultivation and erosion on SOC persistence can only be studied to a limited extent at a broader scale, since their effects are highly context dependent at local scales (Holmes et al., 2004, 2005). Furthermore, the effects of anthropogenic disturbances may be detectable only in the top few centimeters and only for certain soil fractions, such as plant-derived and fast cycling SOC (Heckman et al., 2022; Reichenbach et al., 2023; Rocci et al., 2021). In summary, conclusions about the role of land management practices on

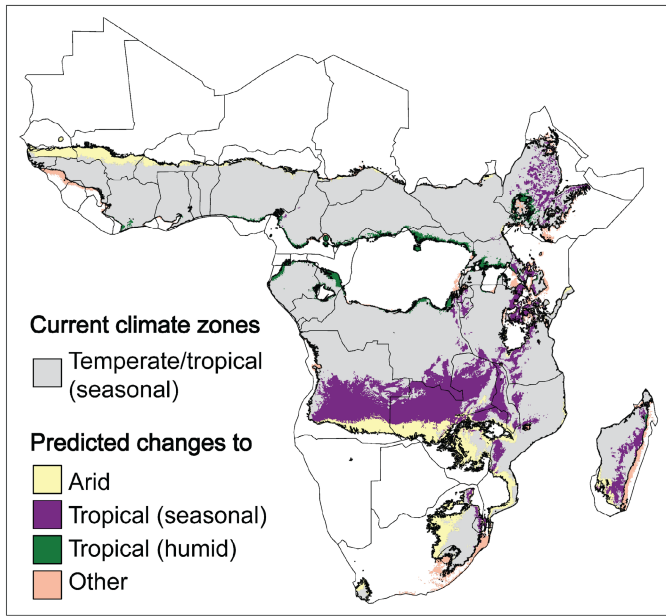
SOC persistence and the exact drivers of the observed differences between natural and degraded soils cannot be drawn from this dataset. At this broad scale, the drivers of degraded soils are likely to be superseded by the effects of the underlying climate and mineralogy on soil C cycling and redistribution.

4.5 | Future scenarios of SOC persistence

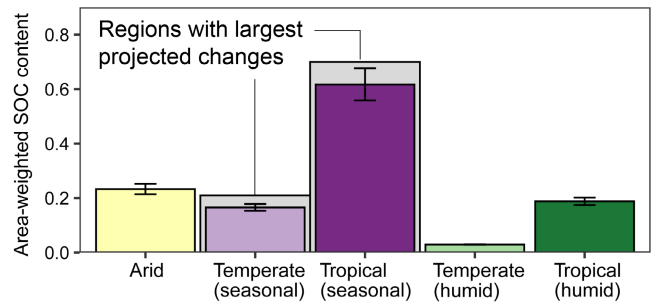
Climate change is projected to have significant effects on the African continent, although predictions have a high level of uncertainty (Lee et al., 2021). Based on CMIP6 projections for the end of this century (RCP8.5, 4°C warming, baseline 1986–2005), sub-Saharan Africa will become warmer (+3 to 4°C) and about 66% of the land area will become wetter, yet with more intense droughts and heavy rainfall events (Gutiérrez et al., 2021; Iturbide et al., 2021). Seasonal climate zones will be subject to the most pronounced climatic changes across sub-Saharan Africa (areas indicated in gray; Figure 6a; Beck et al., 2018; Gutiérrez et al., 2021; Iturbide et al., 2021). Many of these regions will become either more arid (yellow area) or more humid (purple and green area; Figure 6a). For the predicted changes for each climate zone, we used the future climate zones projected by Beck et al. (2018) based on an ensemble of 32 climate model (RCP8.5). Each climate zone is defined according to the Köppen-Geiger classification system, based on threshold values and seasonality of monthly air temperature and precipitation. All of these projected climate changes will have profound impacts on vegetation and soils.

Our results highlight the need to consider the diversity of current pedo-climatic conditions when considering the response of soil C cycling to future changes. For example, the soils from seasonal climates forecast to change most also store the most SOC relative to their area under current climate conditions (Figure 6b), with older soil ages and high C stabilization potential (Figures 3 and 4). These well-developed soils with abundant reactive minerals may have the potential to stabilize more C if plant productivity increases (Figure 6c). The same soils may be less responsive to declining plant productivity if soil minerals can efficiently retain SOC via mineral adsorption (Torn et al., 1997; Figure 6c). In contrast, soil C stocks in predominantly old, deeply weathered soils with younger SOC ages (Figure 5) might not react to climatic changes if biomass productivity continues to exceed the limited capacity of these soils to stabilize C by minerals (Reichenbach et al., 2023; Torn et al., 1997). However, these soils may be very sensitive to decreases in biomass productivity and thus plant C inputs under drier climate conditions (Figure 6c; Feller, 1993; Good & Caylor, 2011). This is because soils of the humid (sub)tropics are already dominated by less reactive 1:1 clays and other end-member minerals that have lost their ability to effectively stabilize SOC by minerals (Figures 3 and 4). Finally, over much longer time periods, climate will impact soil weathering and C stabilization potential. For example, soils that have been constrained by climate in their development to date, such as soils in arid climate zones where lack of water limits chemical weathering and soil stability through

(a) Predicted changes for temperate/tropical (seasonal) climate zones



(b) Mean SOC content across current climate zones



(c) Predicted SOC ages across current climate zones

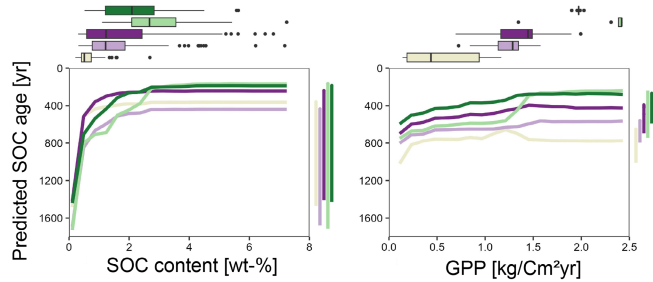


FIGURE 6 (a) Predicted changes in temperate/tropical (seasonal) climate zones by the end of the 21st century based on modeled climate data and the Köppen-Geiger classification system, which uses threshold value and seasonality of monthly air temperature and precipitation (RCP8.5 scenario; Beck et al., 2018). (b) Area-weighted mean soil organic carbon content (SOC) and standard error of the mean for each climate zone. Area-weighted is defined by the proportional area of each climate zone multiplied by the mean SOC content. (c) Individual conditional expectation plots derived from the random forest model grouped by climate zones. Boxplots above the two panels show the raw data distribution for each explanatory variable. Vertical lines next to each panel show the range of the predicted mean SOC ages for each climate zone over the range of one explanatory variable, while holding the other variables constant. Figure shows results for SOC content and gross primary productivity. Map lines delineate study areas and do not necessarily depict accepted national boundaries.

vegetation cover, may develop a more reactive mineral soil phase which would allow them to adsorb more C over longer time periods (Georgiou et al., 2022). These various responses will proceed at different timescales, and future research is needed to connect current pedo-climatic conditions with future soil development to understand projected changes to the soil C cycle over decadal and centennial timescales.

5 | CONCLUSIONS

We show that patterns of SOC persistence are related to common soil development stages, which can be grouped into main pedo-climatic zones at the continental scale for sub-Saharan Africa (Figure 5). Across the diverse soil landscapes of sub-Saharan Africa, our results highlight the varying importance of climate, mineralogy and vegetation as controlling factors for SOC dynamics. This is particularly important as (i) some soils currently have a high potential to stabilize SOC by minerals under the prevailing climatic conditions but will receive either less or more plant C inputs in the future; (ii) soils react more slowly to climatic change than vegetation and (iii) the potential of soils to stabilize SOC on mineral surfaces can change drastically as weathering progresses. At this large scale, anthropogenic alterations of soils through land use

proved less important for understanding patterns of SOC persistence than the underlying pedo-climatic conditions. Furthermore, the results of the linear-mixed effects and random forest models show that we cannot explain all the variation in SOC persistence across sub-Saharan Africa. The unexplained variation may be linked to differences in soil microbiology and soil hydrology for which we did not have data.

Pedo-climatic grouping of soils can be used to inform upscaling efforts to understand broad-scale controls on SOC stocks and timescales of soil C dynamics. It provides a basis for predicting responses of SOC to change. We acknowledge that these predictions remain uncertain. Nevertheless, our results advance our understanding of the very complex soil system at larger scales and call for a more process-oriented grouping and representation of soils in models and upscaling efforts. Besides a better description of climate change effects on vegetation and microbial activity, a pedogenetically informed understanding of the current and future potential of soil C mineral stabilization is crucial for more accurate predictions of the responses of tropical and subtropical soils to climate change.

AUTHOR CONTRIBUTIONS

Sophie F. von Fromm: Conceptualization; data curation; formal analysis; investigation; methodology; visualization; writing – original

draft. **Sebastian Doetterl**: Conceptualization; supervision; writing – review and editing. **Benjamin Butler**: Data curation; formal analysis; methodology; software; writing – review and editing. **Ermias Aynekulu**: Data curation; writing – review and editing. **Asmeret Asefaw Berhe**: Conceptualization; writing – review and editing. **Stephan M. Haefele**: Conceptualization; data curation; funding acquisition; resources; writing – review and editing. **Steve P. McGrath**: Conceptualization; data curation; funding acquisition; resources; writing – review and editing. **Keith D. Shepherd**: Conceptualization; data curation; funding acquisition; resources; writing – review and editing. **Johan Six**: Conceptualization; writing – review and editing. **Lulseged Tamene**: Data curation; resources; writing – review and editing. **Ebagnerin J. Tondoh**: Data curation; resources; writing – review and editing. **Tor-Gunnar Vågen**: Conceptualization; data curation; funding acquisition; resources; writing – review and editing. **Leigh A. Winowiecki**: Conceptualization; data curation; funding acquisition; resources; writing – review and editing. **Susan Trumbore**: Conceptualization; funding acquisition; supervision; writing – review and editing. **Alison Hoyt**: Conceptualization; supervision; writing – review and editing.

ACKNOWLEDGEMENTS

All authors are very grateful to the many people across sub-Saharan Africa who spent countless hours in the field and in the laboratory to collect and analyze the large AfsIS dataset; without these people this work would not have been possible. ST and AH acknowledge support from the European Research Council (Horizon 2020 Research and Innovation Program; grant no. 695101; 14Constraint). The wet chemistry data used in the study was produced by the Chemical and Biological Assessment of AfsIS soils project, which is funded by the Biotechnology and Biological Sciences Research Council (BBSRC)/Global Challenges Research Fund (GCRF; grant no. BBS/OS/GC/000014B). SG and SH were partly funded by the Institute Strategic Program (ISP) grant (Soils to Nutrition—S2N; grant no. BBS/E/C/00010310). The original field surveys and sample analysis costs at ICRAF were covered by the AfsIS Phase I project funded by the Bill and Melinda Gates Foundation (grant no. 51353). SvF received funding from the International Max Planck Research School for Global Biogeochemical Cycles (IMPRS-gBGC). BB acknowledges support from a Macaulay Development Trust Fellowship (United Kingdom, Grant No. MDT-50) and the Scottish Government's Rural and Environment Science and Analytical Services Division. We thank Ulrich Weber for extracting the FLUXCOM data used in this study and Axel Steinhof and his team at the Jena 14C lab for radiocarbon analyses.

CONFLICT OF INTEREST STATEMENT


The authors declare no competing interests.

DATA AVAILABILITY STATEMENT

Wet chemistry data (except for radiocarbon data) is publicly available (<https://doi.org/10.34725/DVN/66BFOB>; Vågen et al., 2021). All data (including radiocarbon data) and R code, necessary to

reproduce the analysis and figures, is publicly available on Github (https://github.com/SophievF/AfsIS_14C). The data that support the findings of this study are in addition openly available in zenodo at <https://doi.org/10.5281/zenodo.10211071> (von Fromm et al., 2023).

ORCID

Sophie F. von Fromm  <https://orcid.org/0000-0002-1820-1455>
 Sebastian Doetterl  <https://orcid.org/0000-0002-0986-891X>
 Benjamin M. Butler  <https://orcid.org/0000-0002-7834-1820>
 Ermias Aynekulu  <https://orcid.org/0000-0002-1955-6995>
 Asmeret Asefaw Berhe  <https://orcid.org/0000-0002-6986-7943>
 Stephan M. Haefele  <https://orcid.org/0000-0003-0389-8373>
 Keith D. Shepherd  <https://orcid.org/0000-0001-7144-3915>
 Johan Six  <https://orcid.org/0000-0001-9336-4185>
 Lulseged Tamene  <https://orcid.org/0000-0002-4846-2330>
 Ebagnerin J. Tondoh  <https://orcid.org/0000-0003-0124-5862>
 Tor-Gunnar Vågen  <https://orcid.org/0000-0002-8699-731X>
 Leigh A. Winowiecki  <https://orcid.org/0000-0001-5572-1284>
 Susan E. Trumbore  <https://orcid.org/0000-0003-3885-6202>
 Alison M. Hoyt  <https://orcid.org/0000-0003-0813-5084>

REFERENCES

- Austin, A. T., & Vivanco, L. (2006). Plant litter decomposition in a semi-arid ecosystem controlled by photodegradation. *Nature*, 442(7102), 555–558. <https://doi.org/10.1038/nature05038>
- Beck, H. E., Zimmermann, N. E., McVicar, T. R., Vergopolan, N., Berg, A., & Wood, E. F. (2018). Present and future Köppen-Geiger climate classification maps at 1-km resolution. *Scientific Data*, 5(1), 180214. <https://doi.org/10.1038/sdata.2018.214>
- Berhe, A. A., Harden, J. W., Torn, M. S., & Harte, J. (2008). Linking soil organic matter dynamics and erosion-induced terrestrial carbon sequestration at different landform positions. *Journal of Geophysical Research: Biogeosciences*, 113(G4). <https://doi.org/10.1029/2008JG000751>
- Bhattacharyya, A., Campbell, A. N., Tfaily, M. M., Lin, Y., Kukkadapu, R. K., Silver, W. L., Nico, P. S., & Pett-Ridge, J. (2018). Redox fluctuations control the coupled cycling of iron and carbon in tropical forest soils. *Environmental Science & Technology*, 52(24), 14129–14139. <https://doi.org/10.1021/acs.est.8b03408>
- Burnham, K. P., & Anderson, D. R. (2002). *Model selection and multimodel inference: A practical information-theoretic approach*. Springer.
- Butler, B. M., & Hillier, S. (2021a). Automated full-pattern summation of X-ray powder diffraction data for high-throughput quantification of clay-bearing mixtures. *Clays and Clay Minerals*, 69(1), 38–51. <https://doi.org/10.1007/s42860-020-00105-6>
- Butler, B. M., & Hillier, S. (2021b). powDR: An R package for quantitative mineralogy using full pattern summation of X-ray powder diffraction data. *Computers & Geosciences*, 147, 104662. <https://doi.org/10.1016/j.cageo.2020.104662>
- Butler, B. M., Palarea-Albaladejo, J., Shepherd, K. D., Nyambura, K. M., Towett, E. K., Sila, A. M., & Hillier, S. (2020). Mineral–nutrient relationships in African soils assessed using cluster analysis of X-ray powder diffraction patterns and compositional methods. *Geoderma*, 375, 114474. <https://doi.org/10.1016/j.geoderma.2020.114474>
- Chen, C., Hall, S. J., Coward, E., & Thompson, A. (2020). Iron-mediated organic matter decomposition in humid soils can counteract protection. *Nature Communications*, 11(1), 2255. <https://doi.org/10.1038/s41467-020-16071-5>
- Chen, L., Fang, K., Wei, B., Qin, S., Feng, X., Hu, T., Ji, C., & Yang, Y. (2021). Soil carbon persistence governed by plant input and mineral

- protection at regional and global scales. *Ecology Letters*, 24(5), 1018–1028. <https://doi.org/10.1111/ele.13723>
- Cusack, D. F., Chadwick, O. A., Hockaday, W. C., & Vitousek, P. M. (2012). Mineralogical controls on soil black carbon preservation. *Global Biogeochemical Cycles*, 26(2). <https://doi.org/10.1029/2011GB004109>
- Cusack, D. F., Chou, W. W., Yang, W. H., Harmon, M. E., Silver, W. L., & Team, T. L. (2009). Controls on long-term root and leaf litter decomposition in neotropical forests. *Global Change Biology*, 15(5), 1339–1355. <https://doi.org/10.1111/j.1365-2486.2008.01781.x>
- Eberl, D. D. (2003). *User's guide to RockJock—A program for determining quantitative mineralogy from powder X-ray diffraction data: Open-File Report 03-78*. U. G. Survey.
- Eglinton, T. I., Eglinton, G., Dupont, L., Sholkovitz, E. R., Montluçon, D., & Reddy, C. M. (2002). Composition, age, and provenance of organic matter in NW African dust over the Atlantic Ocean. *Geochemistry, Geophysics, Geosystems*, 3(8), 1–27. <https://doi.org/10.1029/2001GC000269>
- Feller, C. (1993). Organic inputs, soil organic matter and functional soil organic compartments in low-activity clay soils in tropical zones. In K. Mulongoy & R. Merckx (Eds.), *Soil organic matter and dynamics and sustainability of tropical agriculture* (pp. 77–88). John Wiley & Son.
- Feller, C., & Beare, M. H. (1997). Physical control of soil organic matter dynamics in the tropics. *Geoderma*, 79(1), 69–116. [https://doi.org/10.1016/S0016-7061\(97\)00039-6](https://doi.org/10.1016/S0016-7061(97)00039-6)
- Fick, S. E., & Hijmans, R. J. (2017). WorldClim 2: New 1-km spatial resolution climate surfaces for global land areas. *International Journal of Climatology*, 37(12), 4302–4315. <https://doi.org/10.1002/joc.5086>
- Friedlingstein, P., Jones, M. W., O'Sullivan, M., Andrew, R. M., Bakker, D. C. E., Hauck, J., Le Quéré, C., Peters, G. P., Peters, W., Pongratz, J., Sitch, S., Canadell, J. G., Ciais, P., Jackson, R. B., Alin, S. R., Anthoni, P., Bates, N. R., Becker, M., Bellouin, N., ... Zeng, J. (2022). Global carbon budget 2021. *Earth System Science Data*, 14(4), 1917–2005. <https://doi.org/10.5194/essd-14-1917-2022>
- Friedman, J. H. (2001). Greedy function approximation: A gradient boosting machine. *Annals of Statistics*, 29(5), 1189–1232. <https://doi.org/10.1214/aos/1013203451>
- Gaudinski, J. B., Trumbore, S. E., Davidson, E. A., & Zheng, S. (2000). Soil carbon cycling in a temperate forest: Radiocarbon-based estimates of residence times, sequestration rates and partitioning of fluxes. *Biogeochemistry*, 51(1), 33–69. <https://doi.org/10.1023/A:1006301010014>
- Georgiou, K., Jackson, R. B., Vindušková, O., Abramoff, R. Z., Ahlström, A., Feng, W., Harden, J. W., Pellegrini, A. F. A., Polley, H. W., Soong, J. L., Riley, W. J., & Torn, M. S. (2022). Global stocks and capacity of mineral-associated soil organic carbon. *Nature Communications*, 13(1), 3797. <https://doi.org/10.1038/s41467-022-31540-9>
- Goldstein, A., Kapelner, A., Bleich, J., & Pitkin, E. (2015). Peeking inside the black box: visualizing statistical learning with plots of individual conditional expectation. *Journal of Computational and Graphical Statistics*, 24(1), 44–65. <https://doi.org/10.1080/10618600.2014.907095>
- Good, S. P., & Caylor, K. K. (2011). Climatological determinants of woody cover in Africa. *Proceedings of the National Academy of Sciences of the United States of America*, 108(12), 4902–4907. <https://doi.org/10.1073/pnas.1013100108>
- Gutiérrez, J. M., Jones, R. G., Narisma, G. T., Alves, L. M., Amjad, M., Gorodetskaya, I. V., Grose, M., Klutse, N. A. B., Krakovska, S., Li, J., Martínez-Castro, D., Mearns, L. O., Mernild, S. H., Ngo-Duc, T., van den Hurk, B., & Yoon, J.-H. (2021). Atlas. In V. Masson-Delmotte, P. Zhai, A. Pirani, S. L. Connors, C. Péan, S. Berger, N. Caud, Y. Chen, L. Goldfarb, M. I. Gomis, M. Huang, K. Leitzell, E. Lonnoy, J. B. R. Matthews, T. K. Maycock, T. Waterfield, O. Yelekci, R. Yu, & B. Zhou (Eds.), *Climate change 2021: The physical science basis. Contribution of working group I to the sixth assessment report of the intergovernmental panel on climate change*. Cambridge University Press <http://interactive-atlas.ipcc.ch/>
- Hall, S. J., Berhe, A. A., & Thompson, A. (2018). Order from disorder: Do soil organic matter composition and turnover co-vary with iron phase crystallinity? *Biogeochemistry*, 140(1), 93–110. <https://doi.org/10.1007/s10533-018-0476-4>
- Hall, S. J., & Silver, W. L. (2013). Iron oxidation stimulates organic matter decomposition in humid tropical forest soils. *Global Change Biology*, 19(9), 2804–2813. <https://doi.org/10.1111/gcb.12229>
- Hall, S. J., & Thompson, A. (2022). What do relationships between extractable metals and soil organic carbon concentrations mean? *Soil Science Society of America Journal*, 86(2), 195–208. <https://doi.org/10.1002/saj2.20343>
- Hansen, M. C., Potapov, P. V., Moore, R., Hancher, M., Turubanova, S. A., Tyukavina, A., Thau, D., Stehman, S. V., Goetz, S. J., Loveland, T. R., Kommareddy, A., Egorov, A., Chini, L., Justice, C. O., & Townshend, J. R. G. (2013). High-resolution global maps of 21st-century forest cover change. *Science*, 342(6160), 850–853. <https://doi.org/10.1126/science.1244693>
- Hardy, M., & Cornu, S. (2006). Location of natural trace elements in silty soils using particle-size fractionation. *Geoderma*, 133(3), 295–308. <https://doi.org/10.1016/j.geoderma.2005.07.015>
- Harrison, K. G., Broecker, W. S., & Bonani, G. (1993). The effect of changing land use on soil radiocarbon. *Science*, 262(5134), 725–726. <https://doi.org/10.1126/science.262.5134.725>
- Hassink, J. (1997). The capacity of soils to preserve organic C and N by their association with clay and silt particles. *Plant and Soil*, 191(1), 77–87. <https://doi.org/10.1023/A:1004213929699>
- Heckman, K., Hicks Pries, C. E., Lawrence, C. R., Rasmussen, C., Crow, S. E., Hoyt, A. M., von Fromm, S. F., Shi, Z., Stoner, S., McGrath, C., Beem-Miller, J., Berhe, A. A., Blankinship, J. C., Keiluweit, M., Marin-Spiotta, E., Monroe, J. G., Plante, A. F., Schimel, J., Sierra, C. A., ... Wagai, R. (2022). Beyond bulk: Density fractions explain heterogeneity in global soil carbon abundance and persistence. *Global Change Biology*, 28(3), 1178–1196. <https://doi.org/10.1111/gcb.16023>
- Heckman, K. A., Nave, L. E., Bowman, M., Gallo, A., Hatten, J. A., Matosziuk, L. M., Possinger, A. R., SanClements, M., Strahm, B. D., Weiglein, T. L., Rasmussen, C., & Swanston, C. W. (2021). Divergent controls on carbon concentration and persistence between forests and grasslands of the conterminous US. *Biogeochemistry*, 156(1), 41–56. <https://doi.org/10.1007/s10533-020-00725-z>
- Hengl, T., Heuvelink, G. B. M., Kempen, B., Leenaars, J. G. B., Walsh, M. G., Shepherd, K. D., Sila, A., MacMillan, R. A., Mendes de Jesus, J., Tamene, L., & Tondoh, J. E. (2015). Mapping soil properties of Africa at 250 m resolution: Random forests significantly improve current predictions. *PLoS One*, 10(6), e0125814. <https://doi.org/10.1371/journal.pone.0125814>
- Hijmans, R. J. (2021). *raster: Geographic DATA analysis and modeling*. <https://CRAN.R-project.org/package=raster>
- Holmes, K. W., Kyriakidis, P. C., Chadwick, O. A., Soares, J. V., & Roberts, D. A. (2005). Multi-scale variability in tropical soil nutrients following land-cover change. *Biogeochemistry*, 74(2), 173–203. <https://doi.org/10.1007/s10533-004-3544-x>
- Holmes, K. W., Roberts, D. A., Sweeney, S., Numata, I., Matricardi, E., Biggs, T. W., Batista, G., & Chadwick, O. A. (2004). Soil databases and the problem of establishing regional biogeochemical trends. *Global Change Biology*, 10(5), 796–814. <https://doi.org/10.1111/j.1529-8817.2003.00753.x>
- Iturbide, M., Fernández, J., Gutiérrez, J. M., Bedia, J., Cimadevilla, E., Díez-Sierra, J., Manzanar, R., Casanueva, A., Baño-Medina, J., Milovac, J., Herrera, S., Cofiño, A. S., San Martín, D., García-Díez, M., Hauser, M., Huard, D., & Yelekci, Ö. (2021). *Repository supporting the implementation of FAIR principles in the IPCC-WG1 Atlas* Zenodo. <https://doi.org/10.5281/zenodo.3691645>
- Jackson, M., Tyler, S., Willis, A., Bourbeau, G., & Pennington, R. (1948). Weathering sequence of clay-size minerals in soils and sediments.

- I. Fundamental generalizations. *The Journal of Physical Chemistry*, 52(7), 1237–1260.
- Jones, A., Breuning-Madsen, H., Brossard, M., Dampha, A., Deckers, J., Dewitte, O., Gallali, T., Hallett, S., Jones, R., Kilasara, M., Le Roux, P., Michéli, E., Montanarella, L., Spaargaren, O., Thiombiano, L., van Ranst, E., Yemefack, M., & Zougmore, R. (Eds.). (2013). *Soil atlas of Africa*. Publications Office of the European Union <https://esdac.jrc.ec.europa.eu/content/soil-map-soil-atlas-africa>
- Jung, M., Schwalm, C., Migliavacca, M., Walther, S., Camps-Valls, G., Koirala, S., Anthoni, P., Besnard, S., Bodesheim, P., Carvalhais, N., Chevallier, F., Gans, F., Goll, D. S., Haverd, V., Köhler, P., Ichii, K., Jain, A. K., Liu, J., Lombardozzi, D., ... Reichstein, M. (2020). Scaling carbon fluxes from eddy covariance sites to globe: Synthesis and evaluation of the FLUXCOM approach. *Biogeosciences*, 17(5), 1343–1365. <https://doi.org/10.5194/bg-17-1343-2020>
- Jungkunst, H. F., Göpel, J., Horvath, T., Ott, S., & Brunn, M. (2022). Global soil organic carbon–climate interactions: Why scales matter. *WIREs Climate Change*, 13(4), e780. <https://doi.org/10.1002/wcc.780>
- Kögel-Knabner, I., & Amelung, W. (2021). Soil organic matter in major pedogenic soil groups. *Geoderma*, 384, 114785. <https://doi.org/10.1016/j.geoderma.2020.114785>
- Kassambara, A. (2020). ggpubr: 'ggplot2' based publication ready plots. In (Version R package version 0.4.0). <https://CRAN.R-project.org/package=ggpubr>
- Kassambara, A., & Mundt, F. (2020). *factoextra: Extract and visualize the results of multivariate data analyses*. (Version R package version 1.0.7) <https://CRAN.R-project.org/package=factoextra>
- Keiluweit, M., Bougoure, J. J., Nico, P. S., Pett-Ridge, J., Weber, P. K., & Kleber, M. (2015). Mineral protection of soil carbon counteracted by root exudates. *Nature Climate Change*, 5(6), 588–595. <https://doi.org/10.1038/nclimate2580>
- Khomo, L., Trumbore, S., Bern, C. R., & Chadwick, O. A. (2017). Timescales of carbon turnover in soils with mixed crystalline mineralogies. *The Soil*, 3(1), 17–30. <https://doi.org/10.5194/soil-3-17-2017>
- Lê, S., Josse, J., & Husson, F. (2008). FactoMineR: An R package for multivariate analysis. *Journal of Statistical Software*, 25(1), 1–18. <https://doi.org/10.18637/jss.v025.i01>
- Lal, R. (1985). Soil erosion and sediment transport research in tropical Africa. *Hydrological Sciences Journal*, 30(2), 239–256. <https://doi.org/10.1080/02626668509490987>
- Lang, M., Binder, M., Richter, J., Schratz, P., Pfisterer, F., Coors, S., Au, Q., Casalicchio, G., Kotthoff, L., & Bischl, B. (2019). mlr3: A modern object-oriented machine learning framework in R. *Journal of Open Source Software*, 4(44). <https://doi.org/10.21105/joss.01903>
- Lawrence, C. R., Beem-Miller, J., Hoyt, A. M., Monroe, G., Sierra, C. A., Stoner, S., Heckman, K., Blankinship, J. C., Crow, S. E., McNicol, G., Trumbore, S., Levine, P. A., Vinduškova, O., Todd-Brown, K., Rasmussen, C., Hicks Pries, C. E., Schädel, C., McFarlane, K., Doetterl, S., ... Wagai, R. (2020). An open-source database for the synthesis of soil radiocarbon data: International soil radiocarbon database (ISRaD) version 1.0. *Earth System Science Data*, 12(1), 61–76. <https://doi.org/10.5194/essd-12-61-2020>
- Lee, J.-Y., Marotzke, J., Bala, G., Cao, L., Corti, S., Dunne, J. P., Engelbrecht, F., Fischer, E., Fyfe, J. C., Jones, C., Maycock, A., Mutemi, J., Ndiaye, O., Panickal, S., & Zhou, T. (2021). Future global climate: Scenario-based projections and near-term information. In V. Masson-Delmotte, P. Zhai, A. Pirani, S. L. Connors, C. Péan, S. Berger, N. Caud, Y. Chen, L. Goldfarb, M. I. Gomis, M. Huang, K. Leitzell, E. Lonnoy, J. B. R. Matthews, T. K. Maycock, T. Waterfield, O. Yelekçi, R. Yu, & B. Zhou (Eds.), *Climate change 2021: The physical science basis. Contribution of working group I to the sixth assessment report of the intergovernmental panel on climate change* (pp. 553–672). Cambridge University Press. <https://doi.org/10.1017/9781009157896.006>
- Luo, Z., Viscarra-Rossel, R. A., & Qian, T. (2021). Similar importance of edaphic and climatic factors for controlling soil organic carbon stocks of the world. *Biogeosciences*, 18(6), 2063–2073. <https://doi.org/10.5194/bg-18-2063-2021>
- Martinez, P., & Souza, I. F. (2020). Genesis of pseudo-sand structure in Oxisols from Brazil—A review. *Geoderma Regional*, 22, e00292. <https://doi.org/10.1016/j.geodrs.2020.e00292>
- Masiello, C. A., Chadwick, O. A., Southon, J., Torn, M. S., & Harden, J. W. (2004). Weathering controls on mechanisms of carbon storage in grassland soils. *Global Biogeochemical Cycles*, 18(4). <https://doi.org/10.1029/2004GB002219>
- Mathieu, J. A., Hatté, C., Balesdent, J., & Parent, É. (2015). Deep soil carbon dynamics are driven more by soil type than by climate: A worldwide meta-analysis of radiocarbon profiles. *Global Change Biology*, 21(11), 4278–4292. <https://doi.org/10.1111/gcb.13012>
- Molnar, C. (2022). *Interpretable machine learning: A guide for making black box models explainable* (2nd ed.) <https://christophm.github.io/interpretable-ml-book/>
- Molnar, C., Bischl, B., & Casalicchio, G. (2018). iml: An R package for interpretable machine learning. *Journal of Open Source Software*, 3(26), 786. <https://doi.org/10.21105/joss.00786>
- Nakagawa, S., & Schielzeth, H. (2013). A general and simple method for obtaining R^2 from generalized linear mixed-effects models. *Methods in Ecology and Evolution*, 4(2), 133–142. <https://doi.org/10.1111/j.2041-210x.2012.00261.x>
- Ojanuga, A. G. (1979). Clay mineralogy of soils in the Nigerian Tropical Savanna Regions. *Soil Science Society of America Journal*, 43(6), 1237–1242. <https://doi.org/10.2136/sssaj1979.03615995004300060038x>
- Parfitt, R., & Childs, C. (1988). Estimation of forms of Fe and Al—a review, and analysis of contrasting soils by dissolution and Mossbauer methods. *Soil Research*, 26(1), 121–144. <https://doi.org/10.1071/SR9880121>
- Paul, E. A., Follett, R. F., Leavitt, S. W., Halvorson, A., Peterson, G. A., & Lyon, D. J. (1997). Radiocarbon dating for determination of soil organic matter pool sizes and dynamics. *Soil Science Society of America Journal*, 61(4), 1058–1067. <https://doi.org/10.2136/sssaj1997.03615995006100040011x>
- Pebesma, E. (2018). Simple features for R: Standardized support for spatial vector data. *The R Journal*, 10(1), 439–446. <https://doi.org/10.32614/RJ-2018-009>
- Peterson, R. A., & Cavanaugh, J. E. (2020). Ordered quantile normalization: A semiparametric transformation built for the cross-validation era. *Journal of Applied Statistics*, 47(13–15), 2312–2327. <https://doi.org/10.1080/02664763.2019.1630372>
- Pinheiro, J., Bates, D., DebRoy, S., Sarkar, D., & R Core Team. (2020). *nlme: linear and nonlinear mixed effects models*. (Version R package version 3.1-148) <https://CRAN.R-project.org/package=nlme>
- Polynov, B. B., Muir, A., & Ogg, W. (1937). *The cycle of weathering* (Vol. 1). T. Murby.
- Quéro, S., Hatté, C., Cornu, S., Duviol, A., Cam, N., Jamotteau, F., Borschneck, D., & Basile-Doelsch, I. (2022). Dynamics of carbon loss from an Arenosol by a forest to vineyard land use change on a centennial scale. *The Soil*, 8(2), 517–539. <https://doi.org/10.5194/soil-8-517-2022>
- R Core Team. (2021). *R: A language and environment for statistical computing*. In R Foundation for Statistical Computing. <https://www.R-project.org/>
- Rasmussen, C., Heckman, K., Wieder, W. R., Keiluweit, M., Lawrence, C. R., Berhe, A. A., Blankinship, J. C., Crow, S. E., Druhan, J. L., Hicks Pries, C. E., Marin-Spiotta, E., Plante, A. F., Schädel, C., Schimel, J. P., Sierra, C. A., Thompson, A., & Wagai, R. (2018). Beyond clay: Towards an improved set of variables for predicting soil organic matter content. *Biogeochemistry*, 137(3), 297–306. <https://doi.org/10.1007/s10533-018-0424-3>

- Rasmussen, C., Throckmorton, H., Liles, G., Heckman, K., Meding, S., & Horwath, W. R. (2018). Controls on soil organic carbon partitioning and stabilization in the California Sierra Nevada. *Soil Systems*, 2(3), 41. <https://doi.org/10.3390/soilsystems2030041>
- Reichenbach, M., Fiener, P., Hoyt, A., Trumbore, S., Six, J., & Doetterl, S. (2023). Soil carbon stocks in stable tropical landforms are dominated by geochemical controls and not by land use. *Global Change Biology*, 29(9), 2591–2607. <https://doi.org/10.1111/gcb.16622>
- Rennert, T. (2019). Wet-chemical extractions to characterise pedogenic Al and Fe species—A critical review. *Soil Research*, 57(1), 1–16. <https://doi.org/10.1071/SR18299>
- Rocci, K. S., Lavalley, J. M., Stewart, C. E., & Cotrufo, M. F. (2021). Soil organic carbon response to global environmental change depends on its distribution between mineral-associated and particulate organic matter: A meta-analysis. *Science of the Total Environment*, 793, 148569. <https://doi.org/10.1016/j.scitotenv.2021.148569>
- Sayer, E. J., Lopez-Sangil, L., Crawford, J. A., Bréchet, L. M., Birkett, A. J., Baxendale, C., Castro, B., Rodtassana, C., Garnett, M. H., Weiss, L., & Schmidt, M. W. I. (2019). Tropical forest soil carbon stocks do not increase despite 15 years of doubled litter inputs. *Scientific Reports*, 9(1), 18030. <https://doi.org/10.1038/s41598-019-54487-2>
- Schmidt, M. W. I., Torn, M. S., Abiven, S., Dittmar, T., Guggenberger, G., Janssens, I. A., Kleber, M., Kögel-Knabner, I., Lehmann, J., Manning, D. A. C., Nannipieri, P., Rasse, D. P., Weiner, S., & Trumbore, S. E. (2011). Persistence of soil organic matter as an ecosystem property [perspective]. *Nature*, 478, 49–56. <https://doi.org/10.1038/nature10386>
- Shi, Z., Allison, S. D., He, Y., Levine, P. A., Hoyt, A. M., Beem-Miller, J., Zhu, Q., Wieder, W. R., Trumbore, S., & Randerson, J. T. (2020). The age distribution of global soil carbon inferred from radiocarbon measurements. *Nature Geoscience*, 13(8), 555–559. <https://doi.org/10.1038/s41561-020-0596-z>
- Sierra, C. A., Hoyt, A. M., He, Y., & Trumbore, S. E. (2018). Soil organic matter persistence as a stochastic process: Age and transit time distributions of carbon in soils. *Global Biogeochemical Cycles*, 32(10), 1574–1588. <https://doi.org/10.1029/2018GB005950>
- Sierra, C. A., Müller, M., & Trumbore, S. E. (2014). Modeling radiocarbon dynamics in soils: SoilR version 1.1. *Geoscientific Model Development*, 7(5), 1919–1931. <https://doi.org/10.5194/gmd-7-1919-2014>
- Six, J., Conant, R. T., Paul, E. A., & Paustian, K. (2002). Review: Stabilization mechanisms of soil organic matter: Implications for C-saturation of soils. *Plant and Soil*, 241(2), 155–176. <https://doi.org/10.1023/A:1016125726789>
- Six, J., Elliott, E. T., & Paustian, K. (2000). Soil structure and soil organic matter II. A normalized stability index and the effect of mineralogy. *Soil Science Society of America Journal*, 64(3), 1042–1049. <https://doi.org/10.2136/sssaj2000.6431042x>
- Six, J., Feller, C., Deneff, K., Ogle, S. M., de Moraes Sa, J. C., & Albrecht, A. (2002). Soil organic matter, biota and aggregation in temperate and tropical soils—Effects of no-tillage. *Agronomie*, 22(7–8), 755–775. <https://doi.org/10.1051/agro:2002043>
- Song, X., Wang, P., Van Zwieten, L., Bolan, N., Wang, H., Li, X., Cheng, K., Yang, Y., Wang, M., Liu, T., & Li, F. (2022). Towards a better understanding of the role of Fe cycling in soil for carbon stabilization and degradation. *Carbon Research*, 1(1), 5. <https://doi.org/10.1007/s44246-022-00008-2>
- Steinhof, A. (2013). Data analysis at the Jena 14C laboratory. *Radiocarbon*, 55(2), 282–293. <https://doi.org/10.1017/S0033822200057386>
- Steinhof, A., Altenburg, M., & Machts, H. (2017). Sample preparation at the Jena 14C laboratory. *Radiocarbon*, 59(3), 815–830. <https://doi.org/10.1017/RDC.2017.50>
- Stuiver, M., & Polach, H. A. (1977). Discussion reporting of 14C data. *Radiocarbon*, 19(3), 355–363. <https://doi.org/10.1017/S0033822200003672>
- Tennekes, M. (2018). tmap: Thematic maps in R. *Journal of Statistical Software*, 84(6), 1–39. <https://doi.org/10.18637/jss.v084.i06>
- Terhoeven-Urselmans, T., Vågen, T.-G., Spaargaren, O., & Shepherd, K. D. (2010). Prediction of soil fertility properties from a globally distributed soil mid-infrared spectral library. *Soil Science Society of America Journal*, 74(5), 1792–1799. <https://doi.org/10.2136/sssaj2009.0218>
- Thompson, A., Rancourt, D. G., Chadwick, O. A., & Chorover, J. (2011). Iron solid-phase differentiation along a redox gradient in basaltic soils. *Geochimica et Cosmochimica Acta*, 75(1), 119–133. <https://doi.org/10.1016/j.gca.2010.10.005>
- Tifafi, M., Camino-Serrano, M., Hatté, C., Morras, H., Moretti, L., Barbaro, S., Cornu, S., & Guenet, B. (2018). The use of radiocarbon 14C to constrain carbon dynamics in the soil module of the land surface model ORCHIDEE (SVN r5165). *Geoscientific Model Development*, 11(12), 4711–4726. <https://doi.org/10.5194/gmd-11-4711-2018>
- Tisdall, J. M., & Oades, J. M. (1982). Organic matter and water-stable aggregates in soils. *Journal of Soil Science*, 33(2), 141–163. <https://doi.org/10.1111/j.1365-2389.1982.tb01755.x>
- Torn, M., Trumbore, S., Chadwick, O., Vitousek, P., & Hendricks, D. (1997). Mineral control of soil organic carbon storage and turnover. *Nature*, 389, 170–173. <https://doi.org/10.1038/38260>
- Torn, M. S., Swanston, C. W., Castanha, C., & Trumbore, S. E. (2009). Storage and turnover of organic matter in soil. In *Biophysico-chemical processes involving natural nonliving organic matter in environmental systems* (pp. 219–272). Wiley. <https://doi.org/10.1002/9780470494950.ch6>
- Trumbore, S. (2009). Radiocarbon and soil carbon dynamics. *Annual Review of Earth and Planetary Sciences*, 37(1), 47–66. <https://doi.org/10.1146/annurev.earth.36.031207.124300>
- United Nations. (2022). *World populations prospects 2022: Sub-Saharan Africa total population*. Department of Economic and Social Affairs Population Division.
- Vågen, T.-G., Winowiecki, L. A., Abegaz, A., & Hadgu, K. M. (2013). Landsat-based approaches for mapping of land degradation prevalence and soil functional properties in Ethiopia. *Remote Sensing of Environment*, 134, 266–275. <https://doi.org/10.1016/j.rse.2013.03.006>
- Vågen, T.-G., Winowiecki, L. A., Desta, L., Tondoh, J., Weullow, E., Shepherd, K., Sila, A., Dunham, S. J., Hernández-Allica, J., Carter, J., & McGrath, S. P. (2021). *Wet chemistry data for a subset of AfSIS: Phase I archived soil samples Version V1* [Predicted Wet Chemistry data]. World Agroforestry—Research Data Repository <https://doi.org/10.34725/DVN/66BFOB>
- Vågen, T.-G., Winowiecki, L. A., Tondoh, J. E., Desta, L. T., & Gumbricht, T. (2016). Mapping of soil properties and land degradation risk in Africa using MODIS reflectance. *Geoderma*, 263, 216–225. <https://doi.org/10.1016/j.geoderma.2015.06.023>
- von Fromm, S. F., Doetterl, S., Butler, B., Aynekulu, E., Berhe, A. A., Haefele, S. M., McGrath, S. P., Shepherd, K. D., Six, J., Tamene, L., Tondoh, E. J., Vågen, T.-G., Winowiecki, L. A., Trumbore, S. E., & Hoyt, A. M. (2023). Supporting data for von Fromm et al. (2023) Controls on timescales of soil organic carbon persistence across sub-Saharan Africa [data set]. *Zenodo*. <https://doi.org/10.5281/zenodo.10211071>
- von Fromm, S. F., Hoyt, A. M., Lange, M., Acquah, G. E., Aynekulu, E., Berhe, A. A., Haefele, S. M., McGrath, S. P., Shepherd, K. D., Sila, A. M., Six, J., Towett, E. K., Trumbore, S. E., Vågen, T. G., Weullow, E., Winowiecki, L. A., & Doetterl, S. (2021). Continental-scale controls on soil organic carbon across sub-Saharan Africa. *The Soil*, 7(1), 305–332. <https://doi.org/10.5194/soil-7-305-2021>
- Wang, Y., Amundson, R., & Trumbore, S. (1999). The impact of land use change on C turnover in soils. *Global Biogeochemical Cycles*, 13(1), 47–57. <https://doi.org/10.1029/1998GB900005>
- Wattel-Koekkoek, E. J. W., & Buurman, P. (2004). Mean residence time of kaolinite and smectite-bound organic matter in Mozambiquan soils. *Soil Science Society of America Journal*, 68(1), 154–161. <https://doi.org/10.2136/sssaj2004.1540>
- Wattel-Koekkoek, E. J. W., Buurman, P., van Der Plicht, J., Wattel, E., & van Breemen, N. (2003). Mean residence time of soil organic

- matter associated with kaolinite and smectite. *European Journal of Soil Science*, 54(2), 269–278. <https://doi.org/10.1046/j.1365-2389.2003.00512.x>
- Wickham, H., Averick, M., Bryan, J., Chang, W., D'Agostino McGowan, L., François, R., Grolemund, G., Hayes, A., Henry, L., Hester, J., Kuhn, M., Pedersen, T. L., Miller, E., Bache, S. M., Müller, K., Ooms, J., Robinson, D., Seidel, D. P., Spinu, V., ... Yutani, H. (2019). Welcome to the Tidyverse. *Journal of Open Source Software*, 4(43), 1686. <https://doi.org/10.21105/joss.01686>
- Wickham, H., & Seidel, D. P. (2022). *scales: Scale functions for visualization*. (Version R package version 1.2.1) <https://CRAN.R-project.org/package=scales>
- Wilson, M. J. (1975). Chemical weathering of some primary rock-forming minerals. *Soil Science*, 119(5), 349–355. https://journals.lww.com/soilsci/Fulltext/1975/05000/CHEMICAL_WEATHERING_OF_SOME_PRIMARY_ROCK_FORMING.4.aspx
- Winowiecki, L. A., Vågen, T.-G., & Huising, J. (2016). Effects of land cover on ecosystem services in Tanzania: A spatial assessment of soil organic carbon. *Geoderma*, 263, 274–283. <https://doi.org/10.1016/j.geoderma.2015.03.010>
- Winowiecki, L. A., Vågen, T.-G., Massawe, B., Jelinski, N. A., Lyamchai, C., Sayula, G., & Msoka, E. (2016). Landscape-scale variability of soil health indicators: effects of cultivation on soil organic carbon in the Usambara Mountains of Tanzania. *Nutrient Cycling in Agroecosystems*, 105(3), 263–274. <https://doi.org/10.1007/s10705-015-9750-1>
- Yu, W., Weintraub, S. R., & Hall, S. J. (2021). Climatic and geochemical controls on soil carbon at the continental scale: Interactions and thresholds. *Global Biogeochemical Cycles*, 35(3), e2020GB006781. <https://doi.org/10.1029/2020GB006781>
- Zomer, R. J., Xu, J., & Trabucco, A. (2022). Version 3 of the global aridity index and potential evapotranspiration database. *Scientific Data*, 9(1), 409. <https://doi.org/10.1038/s41597-022-01493-1>
- Zuur, A. F., Ieno, E. N., & Elphick, C. S. (2010). A protocol for data exploration to avoid common statistical problems. *Methods in Ecology and Evolution*, 1(1), 3–14. <https://doi.org/10.1111/j.2041-210X.2009.00001.x>

SUPPORTING INFORMATION

Additional supporting information can be found online in the Supporting Information section at the end of this article.

How to cite this article: von Fromm, S. F., Doetterl, S., Butler, B. M., Aynekulu, E., Berhe, A. A., Haefele, S. M., McGrath, S. P., Shepherd, K. D., Six, J., Tamene, L., Tondoh, E. J., Vågen, T.-G., Winowiecki, L. A., Trumbore, S. E., & Hoyt, A. M. (2023). Controls on timescales of soil organic carbon persistence across sub-Saharan Africa. *Global Change Biology*, 30, e17089. <https://doi.org/10.1111/gcb.17089>